Comparative analysis of silver nanoparticles synthesized by Gram-positive and Gram-negative bacteria: assessing their efficacy in dye removal and antimicrobial activity (#89500)

First revision

Guidance from your Editor

Please submit by **6 Dec 2023** for the benefit of the authors .

Structure and Criteria
Please read the 'Structure and Criteria' page for general guidance.

Raw data check
Review the raw data.

Image check
Check that figures and images have not been inappropriately manipulated.

If this article is published your review will be made public. You can choose whether to sign your review. If uploading a PDF please remove any identifiable information (if you want to remain anonymous).

Files
Download and review all files from the materials page.

1 Tracked changes manuscript(s)
1 Rebuttal letter(s)
9 Figure file(s)
5 Table file(s)
1 Raw data file(s)
1 Other file(s)

Structure and Criteria

Structure your review

The review form is divided into 5 sections. Please consider these when composing your review:

1. **BASIC REPORTING**
2. **EXPERIMENTAL DESIGN**
3. **VALIDITY OF THE FINDINGS**
4. General comments
5. Confidential notes to the editor

You can also annotate this PDF and upload it as part of your review

When ready submit online.

Editorial Criteria

Use these criteria points to structure your review. The full detailed editorial criteria is on your guidance page.

BASIC REPORTING

- Clear, unambiguous, professional English language used throughout.
- Intro & background to show context. Literature well referenced & relevant.
- Structure conforms to PeerJ standards, discipline norm, or improved for clarity.
- Figures are relevant, high quality, well labelled & described.
- Raw data supplied (see PeerJ policy).

EXPERIMENTAL DESIGN

- Original primary research within Scope of the journal.
- Research question well defined, relevant & meaningful. It is stated how the research fills an identified knowledge gap.
- Rigorous investigation performed to a high technical & ethical standard.
- Methods described with sufficient detail & information to replicate.

VALIDITY OF THE FINDINGS

- Impact and novelty not assessed. *Meaningful* replication encouraged where rationale & benefit to literature is clearly stated.
- All underlying data have been provided; they are robust, statistically sound, & controlled.
- Conclusions are well stated, linked to original research question & limited to supporting results.

Standout reviewing tips

The best reviewers use these techniques

Tip	*Example*
Support criticisms with evidence from the text or from other sources	*Smith et al (J of Methodology, 2005, V3, pp 123) have shown that the analysis you use in Lines 241-250 is not the most appropriate for this situation. Please explain why you used this method.*
Give specific suggestions on how to improve the manuscript	*Your introduction needs more detail. I suggest that you improve the description at lines 57- 86 to provide more justification for your study (specifically, you should expand upon the knowledge gap being filled).*
Comment on language and grammar issues	*The English language should be improved to ensure that an international audience can clearly understand your text. Some examples where the language could be improved include lines 23, 77, 121, 128 – the current phrasing makes comprehension difficult. I suggest you have a colleague who is proficient in English and familiar with the subject matter review your manuscript, or contact a professional editing service.*
Organize by importance of the issues, and number your points	*1. Your most important issue* *2. The next most important item* *3. …* *4. The least important points*
Please provide constructive criticism, and avoid personal opinions	*I thank you for providing the raw data, however your supplemental files need more descriptive metadata identifiers to be useful to future readers. Although your results are compelling, the data analysis should be improved in the following ways: AA, BB, CC*
Comment on strengths (as well as weaknesses) of the manuscript	*I commend the authors for their extensive data set, compiled over many years of detailed fieldwork. In addition, the manuscript is clearly written in professional, unambiguous language. If there is a weakness, it is in the statistical analysis (as I have noted above) which should be improved upon before Acceptance.*

Comparative analysis of silver nanoparticles synthesized by Gram-positive and Gram-negative bacteria: assessing their efficacy in dye removal and antimicrobial activity

Bhakti Patel [Equal first author, 1], **Virendra Kumar Yadav** [Equal first author, 1], **Reema Desai** [1], **Shreya Patel** [1], **Abdelfattah Amari** [2], **Nisha Choudhary** [1], **Haitham Osman** [2], **Rajat Patel** [1], **Deepak Balram** [3], **Kuang-Yow Lian** [3], **Dipak Kumar Sahoo** [Corresp., 4], **Ashish Patel** [Corresp. 1]

[1] Department of Life Sciences, Hemchandracharya North Gujarat University, Patan, Gujarat, India

[2] Department of Chemical Engineering, College of Engineering, King Khalid University, Abha, Saudi Arabia

[3] Department of Electrical Engineering, National Taipei University of Technology, Taipei, Taiwan

[4] Department of Veterinary Clinical Sciences, Iowa State University, Ames, Iowa, United States

Corresponding Authors: Dipak Kumar Sahoo, Ashish Patel
Email address: dsahoo@iastate.edu, uni.ashish@gmail.com

In the last decade nanotechnology and nanoparticles have drawn a huge attention of the scientific community in the whole world. The microbial approaches for the synthesis of nanoparticles are more economical, biocompatible, and environment-friendly than the chemical and physical approaches. In the present research work, investigators have synthesized three different types of silver nanoparticles (AgNPs) namely AgNPs-K, AgNPs-M, and AgNPs-E by using *Klebsiella pneumoniae, Micrococcus luteus,* and *Enterobacter aerogenes* respectively. The morphological, chemical, and elemental properties of the synthesized AgNPs were analyzed by using UV-Vis spectroscopy, Fourier transform-infrared spectroscopy (FTIR), X-ray diffraction (XRD), Field emission scanning electron microscope (FESEM) and energy-dispersive spectroscopy (EDX). The UV-Vis spectra show absorbance peaks at 475 nm, 428 nm, and 503 nm for AgNPs synthesized by, *K. pneumoniae, M. luteus,* and *E. aerogenes* respectively. The XRD showed the crystalline nature of the synthesized AgNPs, having peaks at 26.2°, 32.1°, and 47.2°, while the FTIR showed bands at 599 cm^{-1}, 963 cm^{-1}, 1693 cm^{-1}, 2299 cm^{-1}, 2891 cm^{-1}, and at 3780 cm^{-1} for all the types of AgNPs. The FTIR indicated the presence of attached biomolecules from bacteria with developed AgNPs. The size of the silver nanoparticles varies from 10 nm to several microns while the shape varies from spherical to porous sheets-like structure. the percentage of Ag varied from 37.8% (wt.%) to 61.6% i.e., highest in AgNPs-K, and lowest in AgNPs-M. Further, all three types of AgNPs were evaluated for the removal of methyl orange dyes from the simulated wastewater where the maximum dye removal percentage was 19.24% at 120 minutes by AgNPs-M. Finally, all three types of AgNPs were assessed for their potential for antibacterial activity against Gram-positive (*Bacillus subtilis, Bacillus*

cereus, and *Bacillus megaterium*) and Gram-negative bacteria (*Enterococcus fecalis*) out of which the maximum zone of inhibition was 12 mm against *B. megaterium* for the AgNPs-M.

Comparative analysis of silver nanoparticles synthesized by Gram-positive and Gram-negative bacteria: assessing their efficacy in dye removal and antimicrobial activity

Bhakti Patel[1†], Virendra Kumar Yadav[1†], Reema Desai[1], Shreya Patel[1], Abdelfattah Amari[2], Nisha Choudhary[1], Haitham Osman[2], Rajat Patel[1], Deepak Balram[3], Kuang-Yow Lian[3], Dipak Kumar Sahoo[4*], and Ashish Patel[1*]

[1] Department of Life Sciences, Hemchandracharya North Gujarat University, Patan 384265, Gujarat, India

[2]Department of Chemical Engineering, College of Engineering, King Khalid University, Abha 61411, Kingdom of Saudi Arabia

[3] Department of Electrical Engineering, National Taipei University of Technology, No. 1, Section 3, Zhongxiao East Road, Taipei 106, Taiwan

[4] Department of Veterinary Clinical Sciences, College of Veterinary Medicine, Iowa State University, Ames, Iowa, USA

Correspondence: dsahoo@iastate.edu (D.K.S.); uni.ashish@gmail.com (A.P.)

[†] These authors contributed equally to this work.

Abstract

In the last decade nanotechnology and nanoparticles have drawn a huge attention of the scientific community in the whole world. The microbial approaches for the synthesis of nanoparticles are more economical, biocompatible, and environment-friendly than the chemical and physical approaches. In the present research work, investigators have synthesized three different types of silver nanoparticles (AgNPs) namely AgNPs-K, AgNPs-M, and AgNPs-E by using *Klebsiella pneumoniae, Micrococcus luteus,* and *Enterobacter aerogenes* respectively. The morphological, chemical, and elemental properties of the synthesized AgNPs were analyzed by using UV-Vis spectroscopy, Fourier transform-infrared spectroscopy (FTIR), X-ray diffraction (XRD), Field emission scanning electron microscope (FESEM) and energy-dispersive spectroscopy (EDX). The UV-Vis spectra show absorbance peaks at 475 nm, 428 nm, and 503 nm for AgNPs synthesized by, *K. pneumoniae, M. luteus,* and *E. aerogenes* respectively. The XRD showed the crystalline nature of the synthesized AgNPs, having peaks at 26.2°, 32.1°, and 47.2°, while the FTIR showed bands at 599 cm^{-1}, 963 cm^{-1}, 1693 cm^{-1}, 2299 cm^{-1}, 2891 cm^{-1}, and at 3780 cm^{-1} for all the types of AgNPs. The FTIR indicated the presence of attached biomolecules from bacteria with developed AgNPs. The size of the silver nanoparticles varies from 10 nm to several microns while the shape varies from spherical to porous sheets-like structure. the percentage of Ag varied from 37.8% (wt.%) to 61.6% i.e., highest in AgNPs-K, and lowest in AgNPs-M. Further, all three types of AgNPs were evaluated for the removal of methyl orange dyes from the simulated wastewater where the maximum dye removal percentage was 19.24% at 120 minutes by AgNPs-M. Finally, all three types of AgNPs were assessed for their potential for antibacterial activity against Gram-positive (*Bacillus subtilis, Bacillus cereus*, and *Bacillus megaterium*) and Gram-negative bacteria

(*Enterococcus fecalis*) out of which the maximum zone of inhibition was 12 mm against *B. megaterium* for the AgNPs-M.

KEYWORDS silver nanoparticle, methyl orange, bioremediation, antimicrobial, zone of inhibition

1. Introduction

The rapid industrialization in India as well as in the whole world has increased the use of different synthetic dyes (Wang et al., 2023a). Some of the dye may cause harm to aquatic life and cause diseases in living organisms (Patel et al., 2022). Dyes are mainly used in textile industries for coloring fabric, so textile industrial wastewater acts as a major source of dye effluent (Al-Tohamy et al., 2022). The prolonged and continuous mixing of dye-laden water and dye effluents in the freshwater may lead to water pollution (Patel et al., 2022; Agarwal et al., 2022). The consumption of dye-contaminated water may lead to several diseases in humans like skin irritation, and skin cancer in the long term. Dyes present in textile effluent can be removed by using various chemical approaches like precipitation, coagulation (Yadav et al., 2022b; Wang et al., 2023c), flocculation, membrane filtration (nanofiltration, ultrafiltration) (Wang et al., 2020; Chahar et al., 2023; Zhang et al., 2023), reverse osmosis, adsorption, etc. (Robati et al., 2016). The biological approach also involves the utilization of microorganisms for dye remediation, either in the natural sites or in the bioreactor (Das & Mishra, 2017). The biological also involves biosorbents for the remediation of dyes from the wastewater (Cui et al., 2017; Modi et al., 2023). Such processes are economical if the biosorbents are developed from agricultural waste etc. All of these processes have certain advantages and disadvantages but adsorption is a very simple, effective, and economical approach. The adsorbent in the adsorption process could be easily surface functionalized by various chemical compounds for the targeted removal of pollutants (Cui et al., 2013; Chen et al., 2020; Harja, Buema

& Bucur, 2022). The various adsorbents which are commonly used are alumina, silica (Imoisili, Nwanna & Jen, 2022; Yadav et al., 2023), zeolites (Murukutti & Jena, 2022), coal fly ash, magnetite, maghemite, zinc oxide (Soltani et al., 2023), and titanium dioxide (Dash et al., 2018; Yang, Shojaei & Shojaei, 2022) and other complexes (Cui et al., 2017). When these adsorbents are used in their nanoform they become highly effective due to their high surface area to volume ratio (SVR), and high surface energies (Chen et al., 2020; Amari et al., 2023).

Nanotechnology has played an important role in environmental cleanup especially the removal of textile dyes from contaminated water. To date, both metal and metal oxide NPs have been used for dye removal from wastewater and among these silver nanoparticles (AgNPs) (Choudhary, Pathak & Madhusudan, 2017) are widely used. Nanoparticles are materials whose sizes fall in the range of 1 to 100 nm (Puri, Gupta & Mishra, 2021). Due to its high surface area, it has gained huge attention in the field of adsorption-based removal of water pollutants from wastewater. Moreover, NPs have high adsorption capacity due to which dyes easily get adsorbed on the surface of NPs (Wang et al., 2023a). One such NPs is silver nanoparticles (AgNPs) which have antibacterial properties and due to being smaller in size could also act as a nanoadsorbent for the removal of dyes from contaminated water (Dalvand et al., 2020; Degefa et al., 2021; Tarekegn et al., 2021).

AgNPs could be synthesized by all three possible routes i.e., chemical, physical, and biological (Bouafia et al., 2021). The chemical approaches involve chemical coprecipitation, sol-gel, chemical reduction, polyol, etc. Among physical approaches, the most familiar ones are ball milling, vapor condensation method, arc discharge, physical deposition, and laser ablation techniques. The chemical approach involves the utilization of hazardous chemicals, which is not environmental friendly while the physical approach involves the utilization of expensive instruments which makes the synthesis highly expensive. The biological synthesis techniques i.e.,

phytonanofabrication (Choudhary et al., 2023a) and microbial synthesis of AgNPs are of high significance due to the less utilization of chemicals and no requirement of chemical capping agent or surfactant. The microbial synthesis methods provide natural stabilizing and capping agents which make them biocompatible (Naganthran et al., 2022). Among all the microorganisms, bacterial synthesis is preferred due to their easy handling, and short time duration for their growth in comparison to algae and fungi (Wang et al., 2023b; Choudhary et al., 2023b). Bacteria are enriched with several bacterial enzymes and proteins which play crucial roles in the bio-reduction of Ag^{2+} ions into Ag^{0}. These biological molecules act as reducing agents, capping, and stabilizing agents for the developed AgNPs. Vimalanathan and their team synthesized AgNPs by using wet biomass of the *Micrococcus luteus* (Vimalanathan et al., 2013). To date several investigators have used potential bacteria for the synthesis of AgNPs for instance, Esmail and their team reported the synthesis of less than 25 nm AgNPs, by using the supernatant of the bacteria *Bacillus* ROM6. This particular bacterium was isolated from the Zarshouran gold mine, in South Korea. Further, the synthesized AgNPs were used as an antimicrobial agent against *S. aureus*, *E. coli*, *P. aeruginosa*, and *Acinetobacter baumannii* (Esmail et al., 2022).

From the very beginning of civilization, the antimicrobial effect of silver is known due to which it was used for various applications (Kyung et al., 2008). Being a heavy metal, it coagulates the enzymes and proteins of the microorganism, thus inhibiting them and ultimately killing them (Betts, Whitehead & Harris, 2021). So, the nanosized silver can increase the efficiency of antimicrobial activity due to its small size, and high surface area as being smaller in size it may enter the microorganism through the cell wall leading to the inhibition and killing of the microorganism (Karunakaran et al., 2017). Several research studies have revealed that the AgNPs possess incredible antimicrobial activity (Singh & Mijakovic, 2022) which depends upon their

size and surface area (Kalwar & Shan, 2018). The smaller size of AgNPs may facilitate their entry inside the microbes and exhibit their antimicrobial effect. There are several examples where AgNPs have been used as an antimicrobial agent.

Saeed and co-researchers synthesized spherical-shaped AgNPs of size 5-50 nm using bacterial strain; *E. coli*, *Exiguobacterium aurantiacumm*, and *Brevundimonas diminuta*. The investigators further, observed the antimicrobial activity of the synthesized AgNPs against methicillin-resistant *Staphylococcus aureus* (MRSA) and several other multiple drug resistance (MDR) bacteria where the zone of inhibition (ZOI) was varying from 10 mm to 28 mm. Further, the investigators utilized AgNPs against plant pathogens (Saeed, Iqbal & Ashraf, 2020). A team led by Cekuolyte synthesized morphologically different types of AgNPs by using different strains of *Geobacillus* bacteria, namely, 18, 25, 95, and 612 (Cekuolyte et al., 2023). A team led by Raza synthesized AgNPs by using *Aspergillus fumigatus* KIBGE-IB33 and evaluated the antimicrobial activity of AgNPs on the *Enterococcus faecalis* ATCC 29212. Further, the investigators developed a nanocomposite by using the AgNPs with chitosan and observed that the lowest minimum inhibitory concentration of the nanocomposite system was 1.56 µg mL^{-1} against *Enterococcus faecalis* ATCC 29212 (Raza et al., 2021). Srinivasan and their team, synthesized AgNPs by using a bioluminescent bacterium (*Vibrio campbellii*). Further, the investigators assessed the antibacterial and antioxidant activity of the synthesized AgNPs. The antibacterial activity was tested against a number of Gram-negative pathogenic bacteria like *Aeromonas hydrophila* MTCC 1739, *K. pneumoniae* MTCC4030, *Klebsiella oxytoca* MTCC 3030, and *Pseudomonas aeruginosa* MTCC 1934. The AgNPs exhibited antioxidant activity by strong scavenging actions on 2,2-diphenyl-1-picrylhydrazyl (DPPH) (61.88%) and hydrogen peroxide

(53.48%) free radicals (Srinivasan et al., 2022). From the above investigation, it was found that no information on the morphology of AgNPs synthesized by different bacteria. Moreover, AgNPs were used in nanocomposite form so, individual potential assessment of AgNPs. So, a study is needed to investigate the effect on the morphology of AgNPs and purity by different bacteria. Moreover, the antimicrobial effect of morphologically diverse AgNPs on the pathogenic bacteria.

Gola and their group reported the synthesis of 6-25 nm spherical and hexagonal-shaped AgNPs from *Aspergillus sps.* Further, the potential of the myco-synthesized AgNPs was evaluated for the removal of reactive yellow dye and antibacterial effect (Gola et al., 2021). Rasheed and their team synthesized AgNPs from *Conocarpus erectus* and *Pseudomonas* sp. and applied them for the removal of reactive black 5 and reactive red 120 from the aqueous solutions (Rasheed et al., 2023).

In the present research work, investigators have isolated three different bacterial strains from the soil samples. Further, the bacterial strains were used for the synthesis of silver nanoparticles under normal laboratory conditions. The synthesized silver nanoparticles were characterized by Fourier transform infrared spectroscopy, UV-Vis spectroscopy, X-ray diffraction pattern, Field emission scanning electron microscopy, and Energy dispersive X-ray spectroscopy for the confirmation of formation and purity of silver nanoparticles (AgNPs). One of the objectives was to observe the morphological diversity in the synthesized AgNPs by the bacteria. One more objective was to assess the potential of AgNPs as an adsorbent for the remediation of methyl orange dye from the simulated wastewater. One final objective was to evaluate the potential of the synthesized AgNPs as an antibacterial agent against GPB (*B. subtilis, B. cereus, and B. megaterium*) and GNB (*Enterococcus fecalis*).

2. Materials and methods

2.1. Materials

All the bacterial cultures (procured from Gujarat Biotech Research Centre, Gujarat, India), silver nitrate (SRL, Gujarat, India), nutrient agar media (Himedia, Mumbai, India), nutrient broth (Himedia, Gujarat, India), antibiotic assay media (Himedia, Mumbai, India), Ethanol (Shenzhen, China), Whatman filter paper no 42. (Axiva, Mumbai, India), methyl orange (Loba, Chemie, Gujarat, India). All the chemicals were of analytical grade except silver nitrate and Methyl orange dye (LR grade), double distilled water (ddw).

2.2. Methods

2.2.1. Screening and selection of bacteria for the synthesis of AgNPs

Around 10 bacterial colonies were procured on nutrient agar Petri plates which were stored in a refrigerator in the laboratory. Further, about 200 mL nutrient broth was prepared to which about 1 mM aqueous solution of $AgNO_3$ was added. Further, about 10 mL of this mixture was transferred into 10 different Erlenmeyer flasks of 50 mL. To all these flasks a loopful culture of each bacterial strain was added and incubated in an incubator shaker at 37 °C for 2-3 days. After incubation, color change was noticed, and later on, UV-Vis spectra were taken for all the samples. Out of all these bacterial strains only three were found positive for the AgNPs synthesis as color change to red and an absorbance peak near 500-540 nm was observed. So further only these three bacterial strains were used for the mass production of AgNPs. These bacterial strains were identified by 16s rRNA genome sequencing. The selected bacterial strains were *Micrococcus luteus, Klebsiella pneumoniae,* and *Enterobacter aerogenes.*

2.2.2. Synthesis of silver nanoparticles from bacteria

For the fabrication of AgNPs, silver salt was reduced by the bacterial supernatants obtained from all three bacterial strains. The isolated bacterial colonies were grown on nutrient agar plates. Further, for the mass production of each bacterial colonies, a loopful culture was inoculated into the nutrient broth taken in three separate Erlenmeyer flasks. All three flasks containing nutrient broth were incubated in an incubator shaker at 37 ℃ for 24 hours at 120 rpm. Further, after 24 hours, the bacterial colonies were taken out and centrifuged at 5000 rpm for 10 minutes. The bacterial supernatant was retained while the bacterial pellet was discarded. Further, about 100 mL of all three bacterial supernatants were taken separately in three amber bottles, and to each bottle, about 100 mL of silver nitrate solution was added. After that, all three flasks including the control which has ddw instead of bacterial supernatant were kept under dark conditions for 2-3 days, and color change was continuously monitored. Initially, the color of the silver nitrate aqueous solution was pale while, after the addition of bacterial supernatant, the color tuned to milky white in appearance. Finally, after 2-3 days, the color of the three bottles changed from milky white to reddish brown in color indicating the formation of AgNPs. The mixture from each bottle was transferred to the centrifugation tubes separately and centrifuged at 5000 rpm for 10 minutes. The supernatant was discarded while the solid particle was retained. Further, the pellet was washed 2-3 times with distilled water and once with ethanol. All three types of AgNPs were then transferred into different Petri plates and kept for drying in an oven at 50-60 ℃ till complete dryness. **Figure 1** shows the schematic steps involved in the formation of AgNPs from the bacterial supernatant.

FIGURE 1 Schematic diagram for the synthesis of AgNPs using bacterial supernatant.

2.2.3. Preparation of aqueous solution methyl orange dye

A 50-ppm aqueous solution of methyl orange (MO) dye was prepared by adding 50 mg of MO dye powder granules into the 1000 mL ddw. The aqueous solution was kept on a magnetic stirrer along

with vigorous stirring at 250 rpm for the complete dissolution of the dye granules. Further, the aqueous solution was filtered through a Whatman filter paper no 42 in order to remove the impurities. Finally, the dye sample was stored in a an amber colored glass reagent bottle for future use.

2.2.4. Batch study of adsorption of methyl orange dye

About 100 mL of an aqueous solution of MO dye was taken from the stock solution into three different glass beakers of appropriate volume. All these three glass beakers were placed on a magnetic stirrer to which 1 mg AgNPs of each type was added to different glass beakers. The interaction between the AgNPs and MO dye was carried out by agitation at 400 rpm for all three flasks. Further, an aliquot (2-3 mL) was collected from all three glass beakers at 0 minute, 30 mins, 60 mins, 90 mins, and 120 mins. All the collected samples were then analyzed by the UV-Vis spectrophotometer for the concentration of dye samples. The UV-Vis absorbance maxima of MO dye are 520±15 nm. Further, the percentage removal of MO dye was calculated by using the following formula as provided by (Swathilakshmi et al., 2022); -

$$\% \, Dye \, removal = \frac{Co - Ct}{Co} \times 100 \qquad (1)$$

Where, C_o= initial dye concentration,

C_t= dye concentration at a specific time

2.2.5. Antimicrobial activity of silver nanoparticles

The antimicrobial activity of the synthesized AgNPs was checked against *B. subtilis, B. cereus, B. megaterium,* and *E. faecalis* by the disk diffusion method (Yassin et al., 2022). Firstly, 16 disks of

specific size (8 mm diameter) were cut out of filter paper and dipped into separate reagent vials containing AgNPs synthesized from different organisms. Then, all the reagent vials were sonicated for 15-20 minutes using an ultrasonicator (Lequitron). After sonication, the disks were taken out of the vials with the help of forceps and dried in a hot air oven at 40-50 ℃. In the next step, antibiotic assay media was prepared and poured into four petri plates assigned to all four test organisms. Once the media was solidified, the bacterial strains were swabbed in separate petri plates with the help of sterile cotton swabs inside a laminar flow cabinet. The dried AgNPs loaded disks (three disks in one plate) were gently placed on the bacteria-swabbed petri plates. Finally, the Petri plates were placed in a hot air oven/ incubator at 37 ℃ for 24 hours. After 24 hours antibiotic assay plates were observed for the evaluation of antimicrobial activity of the synthesized AgNPs. The ZOI was measured by using a measurement scale against the light and recorded in mm (Ballén et al., 2021).

3. Characterization of silver nanoparticles

3.1. UV-Visible spectroscopy

The UV-Vis measurement of AgNPs was done by dispersing about 1 mg of all three types of AgNPs in 5 mL ddw in three different test tubes. All these three tubes having AgNPs were sonicated in an ultrasonicator (Lequitron) for 10 minutes to disperse the particles. The well-dispersed samples were then taken in a quartz cuvette and the UV-Vis measurement was done in the range of 200-800 nm at a resolution of 1 nm, by using a UV-Vis spectrophotometer (UV 1800, Shimadzu spectrophotometer, Japan).

3.2. FTIR

The FTIR measurement was done to identify the various functional groups present in the bacterially synthesized AgNPs. The FTIR measurement was done by using a solid KBr pellet technique where the pellets were prepared by mixing 2 mg AgNPs and 198 mg KBr for each sample. The FTIR measurement was made in the mid-IR region 599-4000 cm^{-1} at a resolution of 2 cm^{-1} by using a spectrum S6500 instrument (Perkin-Elmer, USA).

3.3. XRD

The XRD patterns for all three types of AgNPs samples were recorded by using Miniflex 800 (Rigaku, Netherlands) instrument equipped X'celerometer in order to reveal the crystallinity. XRD patterns were recorded in the 2-theta range of 20-70 by using a filter K-beta (x1) with a step size of 0.02 and a time of 5 seconds per step, scan speed/duration time: 10.0 degree/min., step width: 0.0200 degree at 30 kV voltage and a current of 2 mA.

3.4. FESEM-EDS

The morphological analysis of all three types of AgNPs was carried out by using a Novo Nanosem, Fei 450, (USA). The dry AgNPs were loaded on the carbon tape with the help of a fine brush which in turn was placed on the aluminum stub holder. All the samples were exposed for gold sputtering. The elemental analysis of AgNPs was analyzed by using an Oxford-made energy-dispersive X-ray spectroscopy (EDS) analyzer attached to the FESEM at variable magnifications and at 20 kV.

4. Results and discussion

4.1. Mechanism of formation of AgNPs by bacteria

The bacterial strains i.e., *K. pneumoniae*, *M. luteus*, and *E. aerogenes* have numerous microbial proteins and enzymes that help in the bioreduction of Ag^{2+} ions into Ag^{0} (Ballén et al., 2021). The

actual mechanism of biosynthesis of AgNPs by bacteria is well described in the literature. It is a very simple and easy mechanism where the oxidized silver ions get two electrons from any of the microbial proteins and enzymes and get reduced to the stabilized Ag^0. When the $AgNO_3$ aqueous solutions are mixed with the bacterial culture or with their supernatant the enzymes and proteins present in the supernatant reduce the Ag^{2+} ions into Ag^0. So, during this step, the previously milky color of the aqueous silver solutions gets converted to red color, which indicates the formation of silver NPs in the medium. Moreover, these biomolecules may also act as stabilizing and capping agents for the synthesized AgNPs (Giri et al., 2022; Terzioğlu et al., 2022). **Figure 2** is showing the mechanism involved in the synthesis of AgNPs from the bacteria. Here the color of the medium changed from milky white to dark brown within 2-3 days. A similar color change (from yellow to brown) was also previously reported by Sayyid and Zghair (2021) during the synthesis of AgNPs by *K. pneumoniae* isolated from humans and sheep (Sayyid & Zghair, 2021). Saleh and Alwan used *K. pneumoniae* culture supernatant for the biosynthesis of AgNPs (Saleh & Khoman Alwan, 2020). Previously Javaid and their team also suggested a similar pathway for the formation of AgNPs from the bacteria via a NADH-dependent nitrate reductase enzyme (Javaid et al., 2018). **Table 1** is showing the major microbial proteins and enzymes present in *K. pneumoniae, M. luteus,* and *E. aerogenes*.

TABLE 1 The major microbial proteins and enzymes present in *K. pneumoniae, M. luteus,* and *E. aerogenes*.

FIGURE 2 Schematic diagram for the formation of AgNPs from silver ions by bacteria via NADH-dependent nitrate reductase enzyme.

4.2. UV-Vis analysis for preliminary confirmation of the formation of AgNPs

Figure 3 shows a typical UV-Vis spectra of AgNPs synthesized by bacteria. All of them exhibit a peak in the range of 425-505 nm. These absorbance peaks indicate the formation of AgNPs from the Ag^{2+} ions by the bacteria (Saleh & Khoman Alwan, 2020). Earlier, Saleh and Alwan (2020) obtained a peak at 432 nm for the AgNPs synthesized by the *K. pneumoniae* (Saleh & Khoman Alwan, 2020), 420 and 440 nm by *M. luteu*s (Vimalanathan et al., 2013), 450 nm by cyanobacterium *Oscillatoria limnetica* (Hamouda et al., 2019), 450 nm by endophytic bacteria *Enterobacter roggenkampii* BLS02 (Kumar & Dubey, 2022), and 405-407 nm for *Klebsiella pneumoniae* by Kalpana and their team. The investigators concluded that when the ratio of $AgNO_3$: bacterial supernatant was about 4:6, then the absorption intensity was higher so they formed AgNPs. Further concluded that the UV–Vis absorption is directly proportional to the amount of substance at their maximum absorption spectra i.e., higher yield of AgNPs and efficient production of AgNPs even at lower concentrations of silver nitrate can be obtained when more amount of cultural filtrate is used. The investigator further also showed that the amount of reducing agents plays an important role in the formation of AgNPs (Kalpana & Lee, 2013).

FIGURE 3 UV-Vis measurement of AgNPs synthesized by bacteria.

4.3. Identification of functional groups of silver NPs by FTIR

A typical FTIR spectra of all the AgNPs (AgNPs-K, AgNPs-M, and AgNPs-E) synthesized by bacteria is shown in **Figure 4** which was used for the identification of various functional groups present AgNPs. All the samples have a common band at 599 cm^{-1} and 963, 1299, 1349, 1693, 2299, 2891, and 3780 cm^{-1}. The band at 599 $cm^{-1}$is attributed to the metallic Ag. The band at 963 $cm^{-1}$is attributed to the amide V band arising due to out-of-plane NH bending of peptide linkages (Kalpana & Lee, 2013). A small intensity band at 1051 $cm^{-1}$is attributed to the primary amine C–N stretch. Another small intensity band at 1349 cm^{-1}in all the samples is attributed to the C-C

bond. A small intensity band in all the samples at 1699 $cm^{-1}$is attributed to the OH group in the samples. Moreover, this band is also attributed to the C=O stretching of amide I bands of peptide linkage. The band at 1229 $cm^{-1}$is attributed to the CN stretching of peptide linkage. The band at 1349 cm^{-1} is attributed to the (C–C) stretching vibration of aliphatic amines., which has earlier also reported by Ibrahim and their team. In their study, the investigators developed AgNPs from endophytic bacteria which showed FTIR band at 1359 cm^{-1} (Ibrahim et al., 2019). All the samples exhibit an atmospheric carbon band at 2891 $cm^{-1}$is attributed to the methylene C–H asymmetric or symmetric stretch. All the samples showing a small band from 3400 $cm^{-1}$to 3800 cm^{-1}centered at 3780 $cm^{-1}$are attributed to the -OH molecule.

Earlier, Saleh and Alwan (2020) obtained four distinct peaks for the AgNPs synthesized by *K. pneumoniae* at 3332.78 cm^{-1}, 2115.35, 1635.60, and 1096.92 cm^{-1}. The investigators concluded that the band obtained at 3332.78 $cm^{-1}$is due to the stretching vibration of the OH bond of alcohol and phenols. The band at 2115.35 $cm^{-1}$was found due to the C-H stretching of the methylene groups of protein and to the N-H stretching of amine salt. The band at 1635.60 $cm^{-1}$was attributed to carbonyl groups (C=O) of the amino acid residues while the band at 1096.92 cm^{-1} was attributed to the (C-O) stretching of alcohols and esters, carboxylic acids, and C–N stretching of aliphatic amines (Saleh & Khoman Alwan, 2020). Based on the above information it was further concluded that the presence of protein in the supernatant acts as a stabilizing and capping agent for stabilization which binds to the synthesized AgNPs through free cysteine or amine groups in proteins (Saleh & Khoman Alwan, 2020). Previously, Kalpana and Lee (2013) also obtained bands for the AgNPs synthesized by using a culture of simulated microgravity-grown *K. pneumoniae*. The investigators obtained major intensity band at 2964.55 cm^{-1}, 1262.22 cm^{-1}, 1095.89 cm^{-1},

1021.96 cm^{-1}, 800.73 cm^{-1}, and small intensity bands at 2960.64 cm^{-1}, 1650.01 cm^{-1}, 865.33 cm^{-1}, 701 $cm^{-1}$and 477.07 cm^{-1}.

FIGURE 4 FTIR spectra of AgNPs synthesized by bacteria.

In the current investigation also, authors have obtained bands for the *K. pneumoniae* synthesized AgNPs at 599, 963, 1229, 1693, 2891, and 3780 cm^{-1} which corresponds to the bands obtained by Kalpana and Lee 2013 (Kalpana & Lee, 2013). A team led by Peiris also obtained four prominent FTIR bands at 1643, 1586, 1397, and 1042 cm^{-1} and concluded that the AgNPs synthesized by bacteria have enhanced stability because of the coating of AgNPs by bacterial and media components (Peiris et al., 2018). AgNPs-M. and AgNPs-E displayed similar bands as that of AgNPs-K with slight variation in their intensity.

4.4. Phase identification of silver nanoparticles by XRD

The XRD investigation was carried out to identify the crystalline phase of the AgNPs. A typical XRD pattern of all the bacterially synthesized AgNPs is shown in **Figure 5**. All the AgNPs exhibit three characteristic peaks of silver NPs at 27.6°, 32.1°, and 46.2°, and three small intensity peaks at 54.7°, and 57.4° and 76.7°. The major intensity peaks in all three types of bacterially synthesized AgNPs are at 32.1° followed by 46.2° and 27.6°. The XRD planes in all three types of AgNPs were 101, 111, 200, 220, and 311 as matched with the Joint Committee on Power Diffraction Standards (JCPDS) 03-0921. In the current investigations, the authors obtained diffraction peaks at 27.6°, 32.1°, and 46.2°, and small diffraction peaks at 54.7°, 57.4° and 76.7° for the AgNPs-K. AgNPs-M has also the same peaks as that of AgNPs-K, i.e., at 27.6, 32.1, 46.2 and 54.7, and 57.4°. All the XRD peaks for AgNPs-M were of almost the same intensity except for 27.6° which was comparatively stronger than the AgNPs-K. The XRD peaks for AgNPs-E were also at the same places as that of AgNPs-M and AgNPs-K, but the peak at 27.6° was of stronger intensity than the

356 AgNPs-K and weaker than the AgNPs-M. Moreover, the peak at 46.2° in both AgNPs-M and
357 AgNPs-E was stronger than the AgNPs-K. Further, the peaks at 54.7° (311) and 57.4° (222) were
358 like a small broad hump in both AgNPs-K and AgNPs-M but these two peaks were sharper in the
359 AgNPs-E.

360 The results were in close agreement with the previous results obtained by Kalpana and Lee (2013)
361 and Ibrahim et al., 2019 where Kalpana and Lee (2013) obtained diffraction peaks at 37.76°, 45.87,
362 64.08°, and 77.11° which was indicated by the (111), (200), (220), and (311) reflection of metallic
363 Ag. The data obtained here was matched with the database of the JCPDS file no 03-0921 (Kalpana
364 & Lee, 2013). Ibrahim and their team obtained diffraction peaks for the AgNPs synthesized by an
365 endophytic bacteria *Bacillus siamensis* strain C1 at 27.81, 32.34, 46.29, 57.47, and 77.69°,
366 corresponding to (101), (111), (200), (220), and (311) crystal planes, respectively, for the AgNPs
367 (Ibrahim et al., 2019). Earlier a team led by Vimalanathan also obtained similar results where the
368 major peaks were at 28, 32, and 47°, and two small intensity peaks at 55° and 57° and a small
369 diffraction peak at 76°.

370 **FIGURE 5** XRD pattern of silver nanoparticles synthesized by bacteria.

371 The crystalline size of the synthesized silver nanoparticle is determined using the Scherrer formula
372 as given in equation (2),

373 $$D = \frac{k\lambda}{\beta \mathrm{Cos}\,\theta} \qquad (2)$$

374 Where,

375 D =crystalline size,

376 k =constant (0.9), and

377 β = the FWHM values of the diffracted peaks.

The highest intensity peak was used to find all the parameters in the Scherrer equation. The Gaussian peak fits were used to find the FWHM values and exact theta values. The calculated crystalline size was found around 16.88 nm, 18.00 nm, and 16.44 nm for AgNPs-K, AgNPs-M, and AgNPs-E. Therefore, it is well examined that the synthesized AgNPs showed a crystalline nature and 16.88 nm, 18.00 nm, and 16.44 nm crystallite size.

4.5. Morphological analysis of silver nanoparticles by FESEM and elemental analysis by EDS

Figure 6a-6f shows FESEM micrographs of AgNPs synthesized by *K. pneumoniae* (AgNPs-K). **Figure 6a&b** show a porous flakes-like structure that is embedded with bright colored AgNPs. **Figure 6c&d** clearly shows rhombohedral-shaped AgNPs, whose size is varying from 22-66 nm. These two images clearly show that the AgNPs are embedded in porous sheet-like structures. **Figure 6e&f** show aggregated spherical-shaped structures. Previously several investigators have shown similar morphology for the bacterially synthesized AgNPs. **Figure 6g** shows the EDS spot of the AgNPs-K while **Figure 6h** exhibits EDS spectra and elemental table of the AgNPs-K. **Figure 6h** shows spectra of Ag, Cl, Na, P, S, C, O, and N. Among these, the elements contributing highest to the sample were; Ag (37.8% At wt.), Cl (29.8%), Na (21.8) C (7 %), and O (2.8%). The rest of the identified elements i.e., P, S and N were not detected in the AgNPs-K. The major impurities in the synthesized AgNPs-K are NaCl which alone comprises 50% this indicates the improper washing of the samples. Moreover, these two may also come from the nutrient broth used for growing the bacteria. While the presence of C, S, and P indicates the presence of biomolecules with the synthesized AgNPs-K. Earlier Sayyid and Zghair (2021) reported cube-shaped to irregular heterogeneous forms of AgNPs synthesized by *K. pneumoniae* whose average size was 40.47 nm (Sayyid & Zghair, 2021). Moreover, investigators further observed that the morphology by TEM was a pseudo-spherical shape of size 40-80 nm.

FIGURE 6 FESEM images (a-f), EDS spot (g), and EDS spectra and elemental table (h) for AgNPs-K. FESEM images (i-l), EDS spot (m) and EDS spectra, and elemental table (n) for AgNPs-M. FESEM images (o-r), EDS spot (s) and EDS spectra, and elemental table (t) for AgNPs-E.

Saleh and Alwan (2020) obtained spherical-shaped particles of size 26.84 to 44.42 nm which were highly aggregated. Further, the investigators concluded the conglomeration of the AgNPs is during the drying process (Saleh & Khoman Alwan, 2020).

Figure 6i-l shows FESEM micrographs of AgNPs synthesized by the *M. luteus* (AgNPs-M). **Figure 6i&j** shows a high aggregation of the synthesized AgNPs-M. **Figure 6k** and **Figure 6l** show spherical-shaped AgNPs-M whose size is varying from 21-45 nm. **Figure 6m** shows the EDS spot of the AgNPs-M while **Figure 6n** exhibits EDS spectra and elemental table of the AgNPs-M. The EDS spectra of AgNPs-M in **Figure 6n** show peaks for Ag, Cl, Na, P, S, C, O, and N. Out of all these the major elements were mainly Ag (61% At wt.), Cl (21%), C (8.4%), N (3.7%) and O (2.6%). Other detected elements such as Na, P, and S were present in trace amounts. The major impurity in the final sample was Cl which is due to improper washing of the sample. Moreover, it also came from the bacterial media i.e., nutrient broth. While the presence of C, N, S, and P indicates the presence of biomolecules with the AgNPs-M.

Figure 6o-r shows FESEM micrographs of AgNPs synthesized by *E. aerogenes* (AgNPs-E). **Figure 6o&p** shows a porous flakes-like structure that is embedded with the bright color of AgNPs. **Figure 6q&r** clearly show rhombohedral-shaped AgNPs-E, whose size is varying from 24-60. The images clearly shows that the AgNPs-E are embedded in the porous flakes-like structures. The particles are showing high aggregation as evident from the images. **Figure 6s** shows the EDS spot of the AgNPs-E while **Figure 6t** exhibits EDS spectra and elemental table of

the AgNPs-E. **Figure 6t** shows spectra of Ag, Cl, Na, P, S, C, O, and N. Out of all these the major elements were mainly Ag (52.1% At wt.), Cl (21.7%), C (9.8 %) and O (8.2%), Na (4.0%) and N (3.1%). In addition to this P and S were present in trace amounts whose total composition was near 1.1%. The major impurities in the synthesized AgNPs-E are NaCl which alone comprises 25.7% which indicates the improper washing of the sample. Moreover, these two may also come from the nutrient broth used for growing the bacteria. While the presence of C, S, N, and P indicates the presence of biomolecules with the synthesized AgNPs-E. **Table 2** shows the major elements present with all three types of AgNPs synthesized by bacteria.

TABLE 2 Comparison between all the elements present in all three types of AgNPs.

From the EDS data of all three types of AgNPs, it was found that Ag was present in the highest percentage in AgNPs-M while at least 37.8% in AgNPs-K. Among all the three types of AgNPs, Cl was present maximum in AgNPs-K while least in AgNPs-M (21.0%). The oxygen was present in the highest amount in AgNPs-E and the least in AgNPs-K i.e., 8.2% and 2.8% respectively. The carbon was highest in AgNPs-E (9.8%) and least 7.0% in AgNPs-K. Out of all the three types of AgNPs, Na was highest in AgNPs-K (21.8%) and least in AgNPs-M (0.4%). Among all the three samples of AgNPs, N was present highest in AgNPs-M (3.7%) and 3.1% in AgNPs-E and it was not detected in AgNPs-K. The P and S were present almost similar in all the samples but least in AgNPs-K i.e., 0.4%.

In the current investigation, the authors have got a broad peak of silver ions at 3 keV in all three types of AgNPs, which confirmed the reduction of Ag^{+} to Ag^{0}. Moreover, here the authors have mainly got peaks in EDS for Ag, Cl, and carbon. The peaks for Ag, Cl, and S were consistent with the results obtained for the AgNPs synthesized by endophytic bacteria by Ibrahim and their team. Ibrahim and their team also concluded that the broad peak of silver ions was formed at 3 keV,

447 which indicated the reduction of Ag^{2+} to Ag^{0} (Ibrahim et al., 2019). **Table 3** shows the comparative
448 analysis of all the previously reported the bacterially synthesized AgNPs with the current
449 investigation.

450 **TABLE 3 The comparative analysis of all the previous study and current investigation of the**
451 **bacterially synthesized AgNPs.**

452 From all the previous investigations, it was revealed that the largest size of AgNPs was 40.47±89
453 nm synthesized by using *K. pneumoniae* whose shape was cube to spherical. The smallest AgNPs
454 were synthesized by *B. cereus* whose size was 2-16 nm and spherical shaped. In the current
455 investigation, the size of the synthesized AgNPs varied from 21 nm to 66 nm. Earlier three more
456 investigators synthesized AgNPs from different species of *Klebsiella pneumoniae* which were
457 mainly spherical shaped and cube-shaped. Except in one or two cases most of the synthesized
458 AgNPs were spherical in shape whereas in two cases cube shaped AgNPs were obtained. In terms
459 of elemental composition and purity AgNPs synthesized by *B. siamensis* strain C1 were purest
460 where Ag was 91.8% while the remaining was impurity mainly by Cl and S, whereas in our case
461 the Ag percentage varied from 37.8% to 61.6% i.e., less than the earlier reported by Ibrahim and
462 their team. The lower purity could be due to improper washing of the AgNPs during centrifugation.
463 From the UV-Vis study, it was found that the absorbance peak of AgNPs synthesized from
464 different bacteria could be varied from 400 to 510 based on the size and shape of the synthesized
465 AgNPs. From XRD and FTIR, it was found that the majority of the peaks and bands remain the
466 same in all the syntheses with slight variations respectively.

467 **4.6. Batch adsorption study of methyl orange dye by AgNPs**

MO dye shows the highest absorbance at 464 nm when examined using a UV-Vis spectrophotometer. The AgNPs-M, AgNPs-K, and AgNPs-E treated MO were measured for their color intensity in an aqueous dye solution up to a time of 120 mins at a regular interval of 30 mins. With passing time, the concentration of MO dye in the sample decreased gradually which is evident from the UV-visible spectra (Figure 7 a, b, and c). So, the maximum removal of MO dye was found after 120 mins using AgNPs-M. The readings at an interval of every 30 mins show a slow decrease in the concentration and absorbance of the dye, hence the decrease in the graph can be observed easily as moves from 0 min to 120 mins. **Figure 7 a, b, and c** shows the MO dye absorbance by UV-Vis spectroscopy at different time intervals.

FIGURE 7 MO dye removal by different types of AgNPs with respect to contact time as measured by UV-Vis spectrophotometer: a) AgNPs-K, b) AgNPs-M, and c) AgNPs-E.

4.7. Percentage removal of MR dye by all the AgNPs

AgNPs-M removed MO dye 2.34% at 30 min, 4.37% at 60 min, 14.83% at 90 min, and 19.24% at 120 min. AgNPs-K removes MO dye 1.50% at 30 min, 4.06% at 60 min, 9.56% at 90 min, and 15.03% at 120 min. AgNPs-E removes MO dye 1.52% at 30 min, 2.36% at 60 min, 3.86% at 90 min, and 4.15% at 120 min. By comparing all the AgNPs mention above we can observe that AgNP-M has more efficiency of dye removal and AgNPs-E have the least efficiency of dye removal. **Figure 8** shows the percentage removal of MO dye by all three types of AgNPs.

FIGURE 8 Percentage removal of MO dye by all three types of AgNPs.

Earlier Gola and their team photocatalytically degraded the reactive yellow dye from the aqueous solution by using AgNPs synthesized by *Aspergillus sps*. Here the initial dye concentration was about 20-100 mg/L, where about 1 g/L retentate biomass of the fungus removed 82-100% dye

490 respectively. As the initial dye concentration was increased the decolorization efficiency of the
491 biomass retentate was decreased from 9.2% to 32.3% (Gola et al., 2021). Rasheed and their team,
492 removed reactive black 5 and reactive red 120 dye from the aqueous solutions (<90%) by using
493 AgNPs synthesized from *C. erectus* and a bacterial strain *Pseudomonas* sp. The bacterially
494 synthesized AgNPs showed greater removal of both dyes in comparison to the chemically
495 synthesized AgNPs (Rasheed et al., 2023). Earlier Batool and their team reported the synthesis of
496 AgNPs from *Salvinia molesta* and used them for the removal of methylene blue from the aqueous
497 solution d where the highest adsorption capacity of the dye on the surface of AgNPs was 121.04
498 mg/g by the Langmuir isotherm (Batool, Daoush & Hussain, 2022). Bhankhar and their group
499 removed MO up to 83% by using chemically synthesized AgNPs in the presence of $NaBH_4$ under
500 optimized conditions (Bhankhar et al., 2014).

501 **4.8. Antimicrobial activity of the synthesized AgNPs**

502 AgNPs-K shows a ZOI of 11 mm against *B. megaterium* and *E. fecalis*. *B. subtilis* shows a
503 moderate ZOI of 10 mm when compared with other zones, and *B. cereus* shows a 9 mm ZOI due
504 to the effect of AgNP.s

505 Earlier Syyaid and Zghair also used the *K. pneumoniae* synthesized AgNPs for the antimicrobial
506 activity against *S. aureus* and *Escherichia coli*. The investigators used about 40-50 µg/mL of
507 AgNPs and found that *E. coli* was more susceptible to AgNPs compared to Gram-positive bacteria
508 such as *S. aureus*. Further, the investigators suggested that this could be due to variations in the
509 thickness and composition of their cell walls, like peptidoglycan (Sayyid & Zghair, 2021). Saleh
510 and Alwanz (2020) assessed the three concentrations of AgNPs (50, 10, and 150 µg/mL)
511 synthesized from *K. pneumoniae* and evaluated them against *E. coli, P. aeruginosa, Staph. aureus,*
512 *and B. cereus*. Investigators reported that the highest concentration i.e., 150 µg/mL was found

most effective against these pathogens in comparison to the 50 and 100 µg/mL. This suggests that the increase in the concentration of AgNPs increases the antibacterial activity (Saleh & Khoman Alwan, 2020).

The use of AgNPs-M for antibacterial activity using different bacteria like *B. subtilis, B. cereus, B. megaterium, E. fecalis* shows different ZOI. AgNPs-M shows a maximum ZOI of 12 mm against *B. megaterium* and a minimum ZOI against *B. cereus* of 8 mm. It shows a moderate ZOI of 9 mm against *E. fecalis* and 11 mm against *B. subtilis***.** The *B. megaterium* was more susceptible than *E. fecalis* and *B. subtilis* moderately susceptible, and *B. cereus* was less susceptible to the AgNPs-M. *B. cereus* gives a greater ZOI of 11 mm due to the effect of AgNPs-E the lowest ZOI is observed against *B. megaterium* which is 8 mm and also shows a 10 mm ZOI by *B. subtilis and E. fecalis.*

Previously a team led by Gola obtained a ZOI of about 13 and 10 mm against *E. coli* and *S. aureus* respectively for the AgNPs synthesized by *Aspergillus sps.* Further, the investigator evaluated the synergistic effect of AgNPs and penicillin against *E. coli* and *S. aureus* and showed 0.49- and 0.36-fold increases in the ZOI respectively in comparison to the AgNPs and penicillin alone (Gola et al., 2021).

Figure 9 shows the antibacterial activity of Petri plates of the AgNPs against tested bacterial species. **Table 4** shows the ZOI, tested bacterial species, and AgNPs, while, **Table 5** shows comparison of antibacterial activity of current investigation with previously reported studies.

FIGURE 9 Antibacterial activity, zone of inhibition of AgNPs synthesized against the tested bacterial species.

TABLE 4 The ZOI, tested bacterial species, against different bacterially synthesized AgNPs.

TABLE 5 Summarized form of comparison of antibacterial activity of AgNPs of earlier reported work and current investigation.

The difference between the antibacterial effect against GPB and GNB bacteria over here might be due to the morphological differences in both types of bacteria (Jubeh, Breijyeh & Karaman, 2020). GPB have a thick peptidoglycan layer while GNB have a thin peptidoglycan layer but a thick lipopolysaccharide layer (Pasquina-Lemonche et al., 2020). A similar reason was also given by several other investigators for the antimicrobial activity of the synthesized AgNPs (Kalpana & Lee, 2013). Investigators reported that spherical AgNPs have higher antibacterial/antimicrobial activity due to high SVR (Al-Ogaidi & Rasheed, 2022). Moreover, due to their large surface area, they could bind with various ligands. AgNPs can easily infiltrate the bacterial cell membrane and that is the reason for their enhanced antimicrobial activity which might improve more with a further decrease in the size of AgNPs (Anees Ahmad et al., 2020; Wypij et al., 2021). AgNPs get attached to the cell membrane where it releases Ag ions slowly. Further, AgNPs are reported to develop pits in the cell wall of microorganisms which leads to enhanced permeability and leakage of cellular components through the plasma membrane (Tripathi et al., 2017; Matras et al., 2022).

5. Conclusions

The present research was conducted to check the potential of microorganisms isolated from contaminated sites such as industrial areas, for nanoparticle synthesis and application of such nanoparticles in the removal of contaminants like synthetic dye compounds which are manufactured in such industries. Microorganisms that are indigenously found in such contaminated environments have a natural capability of degrading the contaminants present there. So, here the authors have successfully synthesized silver nanoparticles of different shapes and sizes by using different bacterial strains (containing different types of microbial proteins and enzymes)

obtained from contaminated sites in the Gujarat region of India. The variations in the microbial proteins and enzymes help in determining the morphology of the silver nanoparticles. The microscopic techniques confirm the spherical shape of AgNPs, while EDS shows the purity of the AgNPs. The XRD exhibited the crystalline nature of the AgNPs, while FTIR showed the typical IR bands for the AgNPs. FTIR also showed the presence of organic biomolecules with the synthesized AgNPs. The methyl orange dye removal percentage for the AgNPs was highest up to 20% with AgNPs-M. While the highest antibacterial activity was exhibited with AgNPs-M against *B. megaterium* i.e., 12 mm.

Funding: This research was funded by the Deanship of Scientific Research at King Khalid University under the grant number R.G.P. 2/174/44.

Acknowledgements: The authors extend their appreciation to the Deanship of Scientific Research at King Khalid University for supporting this research work. The authors are also thankful to Department of Life Sciences, Hemchandracharya North Gujarat University for providing the lab facilities.

References

Agarwal N, Solanki VS, Gacem A, Hasan MA, Pare B, Srivastava A, Singh A, Yadav VK, Yadav KK, Lee C, Lee W, Chaiprapat S, Jeon BH. 2022. Bacterial Laccases as Biocatalysts for the Remediation of Environmental Toxic Pollutants: A Green and Eco-Friendly Approach—A Review. *Water* 14:4068. DOI: 10.3390/w14244068.

580 Al-Ogaidi MAZ, Rasheed BG. 2022. Enhancement of Antimicrobial Activity of Silver
581 Nanoparticles Using Lasers. *Lasers in Manufacturing and Materials Processing* 9:610–621.
582 DOI: 10.1007/s40516-022-00192-4.

583 Al-Tohamy R, Ali SS, Li F, Okasha KM, Mahmoud YA-G, Elsamahy T, Jiao H, Fu Y, Sun J.
584 2022. A critical review on the treatment of dye-containing wastewater: Ecotoxicological and
585 health concerns of textile dyes and possible remediation approaches for environmental
586 safety. *Ecotoxicology and Environmental Safety* 231:113160. DOI:
587 https://doi.org/10.1016/j.ecoenv.2021.113160.

588 Amari A, Yadav VK, Pathan SK, Singh B, Osman H, Choudhary N, Khedher KM, Basnet A.
589 2023. Remediation of Methyl Red Dye from Aqueous Solutions by Using Biosorbents
590 Developed from Floral Waste. *Adsorption Science & Technology* 2023:1–17. DOI:
591 10.1155/2023/1532660.

592 Anees Ahmad S, Sachi Das S, Khatoon A, Tahir Ansari M, Afzal Mohd, Saquib Hasnain M,
593 Kumar Nayak A. 2020. Bactericidal activity of silver nanoparticles: A mechanistic review.
594 *Materials Science for Energy Technologies* 3:756–769. DOI:
595 https://doi.org/10.1016/j.mset.2020.09.002.

596 Ballén V, Gabasa Y, Ratia C, Ortega R, Tejero M, Soto S. 2021. Antibiotic Resistance and
597 Virulence Profiles of Klebsiella pneumoniae Strains Isolated From Different Clinical
598 Sources. *Frontiers in Cellular and Infection Microbiology* 11.

599 Batool M, Daoush WM, Hussain MK. 2022. Dye Sequestration Using Biosynthesized Silver
600 Nanoparticles Adsorbent in Aqueous Solutions. *Crystals* 12. DOI: 10.3390/cryst12050662.

601 Betts HD, Whitehead C, Harris HH. 2021. Silver in biology and medicine: opportunities for
602 metallomics researchers. *Metallomics* 13:mfaa001. DOI: 10.1093/mtomcs/mfaa001.

603 Bhankhar A, Giri M, Yadav K, Jaggi N. 2014. Study on degradation of methyl orange-an azo dye
604 by silver nanoparticles using UV-Visible spectroscopy. *Indian Journal of Physics* 88:1191–
605 1196. DOI: 10.1007/s12648-014-0555-x.

606 Bouafia A, Laouini SE, Ahmed ASA, Soldatov A V., Algarni H, Chong KF, Ali GAM. 2021. The
607 recent progress on silver nanoparticles: Synthesis and electronic applications. *Nanomaterials*
608 11. DOI: 10.3390/nano11092318.

609 Cekuolyte K, Gudiukaite R, Klimkevicius V, Mazrimaite V, Maneikis A, Lastauskiene E. 2023.
610 Biosynthesis of Silver Nanoparticles Produced Using Geobacillus spp. Bacteria.
611 *Nanomaterials* 13. DOI: 10.3390/nano13040702.

612 Chahar M, Khaturia S, Singh HL, Singh Solanki V, Agarwal N, Sahoo K, Yadav VK, Patel A.
613 2023. Recent advances in the effective removal of hazardous pollutants from wastewater by
614 using nanomaterials-A review. *Front. Environ. Sci.* 11. DOI: 10.3389/fenvs.2023.1226101.

615 Chen D, Wang Q, Li Y, Li Y, Zhou H, Fan Y. 2020. A general linear free energy relationship for
616 predicting partition coefficients of neutral organic compounds. *Chemosphere* 247:125869.
617 DOI: https://doi.org/10.1016/j.chemosphere.2020.125869.

618 Choudhary N, Chaudhari J, Mochi V, Patel P, Ali D, Alarifi S, Sahoo DK, Patel A, Kumar Yadav
619 V. 2023a. Phytonanofabrication of Copper Oxide by Albizia saman and Their Potential as
620 an Antimicrobial Agent and Remediation of Congo Red Dye from Wastewater. *Water*
621 15:3787. DOI: 10.3390/w15213787.

622 Choudhary N, Dhingra N, Gacem A, Yadav VK, Verma RK, Choudhary M, Bhardwaj U,
623 Chundawat RS, Alqahtani MS, Gaur RK, Eltayeb LB, Al Abdulmonem W, Jeon B-H. 2023b.
624 Towards further understanding the applications of endophytes: enriched source of bioactive
625 compounds and bio factories for nanoparticles. *Frontiers in Plant Science* 14. DOI:
626 10.3389/fpls.2023.1193573.

627 Choudhary N, Pathak B, Madhusudan HF. 2017. Antimicrobial Potential of Green Synthesized
628 Silver nanoparticles using Sida acuta Leaf extract. *Nano Science & Nano Technology: An*
629 *Indian Journal Research* 11:111–1120.

630 Cui G, Bai Y, Li W, Gao Z, Chen S, Qiu N, Satoh T, Kakuchi T, Duan Q. 2017. Synthesis and
631 characterization of Eu(III) complexes of modified d-glucosamine and poly(N-
632 isopropylacrylamide). *Materials Science and Engineering: C* 78:603–608. DOI:
633 https://doi.org/10.1016/j.msec.2017.03.059.

634 Cui G, Li Y, Shi T, Gao Z, Qiu N, Satoh T, Kakuchi T, Duan Q. 2013. Synthesis and
635 characterization of Eu(III) complexes of modified cellulose and poly(N-
636 isopropylacrylamide). *Carbohydrate Polymers* 94:77–81. DOI:
637 https://doi.org/10.1016/j.carbpol.2013.01.045.

638 Dalvand R, Kianpour E, Tahzibi H, Azizian S. 2020. MgO nano-sheets for adsorption of anionic
639 dyes from aqueous solution: Equilibrium and kinetics studies. *Surfaces and Interfaces*
640 21:100722. DOI: https://doi.org/10.1016/j.surfin.2020.100722.

641 Das A, Mishra S. 2017. Removal of textile dye reactive green-19 using bacterial consortium:
642 Process optimization using response surface methodology and kinetics study. *Journal of*

643 *Environmental Chemical Engineering* 5:612–627. DOI:
644 https://doi.org/10.1016/j.jece.2016.10.005.

645 Dash S, Chaudhuri H, Gupta R, Nair UG. 2018. Adsorption study of modified coal fly ash with
646 sulfonic acid as a potential adsorbent for the removal of toxic reactive dyes from aqueous
647 solution: Kinetics and thermodynamics. *Journal of Environmental Chemical Engineering*
648 6:5897–5905. DOI: https://doi.org/10.1016/j.jece.2018.05.017.

649 Degefa A, Bekele B, Jule LT, Fikadu B, Ramaswamy S, Dwarampudi LP, Nagaprasad N,
650 Ramaswamy K. 2021. Green Synthesis, Characterization of Zinc Oxide Nanoparticles, and
651 Examination of Properties for Dye-Sensitive Solar Cells Using Various Vegetable Extracts.
652 *Journal of Nanomaterials* 2021. DOI: 10.1155/2021/3941923.

653 Esmail R, Afshar A, Morteza M, Abolfazl A, Akhondi E. 2022. Synthesis of silver nanoparticles
654 with high efficiency and stability by culture supernatant of Bacillus ROM6 isolated from
655 Zarshouran gold mine and evaluating its antibacterial effects. *BMC Microbiology* 22. DOI:
656 10.1186/s12866-022-02490-5.

657 Giri AK, Jena B, Biswal B, Pradhan AK, Arakha M, Acharya S, Acharya L. 2022. Green synthesis
658 and characterization of silver nanoparticles using Eugenia roxburghii DC. extract and
659 activity against biofilm-producing bacteria. *Scientific Reports* 12:8383. DOI:
660 10.1038/s41598-022-12484-y.

661 Gola D, Tyagi PK, Arya A, Gupta D, Raghav J, Kaushik A, Agarwal M, Chauhan N, Srivastava
662 SK. 2021. Antimicrobial and dye degradation application of fungi-assisted silver
663 nanoparticles and utilization of fungal retentate biomass for dye removal. *Water*
664 *Environment Research* 93:2727–2739. DOI: https://doi.org/10.1002/wer.1629.

665 Hamouda RA, Hussein MH, Abo-elmagd RA, Bawazir SS. 2019. Synthesis and biological
666 characterization of silver nanoparticles derived from the cyanobacterium Oscillatoria
667 limnetica. *Scientific Reports* 9:13071. DOI: 10.1038/s41598-019-49444-y.

668 Harja M, Buema G, Bucur D. 2022. Recent advances in removal of Congo Red dye by adsorption
669 using an industrial waste. *Scientific Reports* 12:6087. DOI: 10.1038/s41598-022-10093-3.

670 Ibrahim E, Fouad H, Zhang M, Zhang Y, Qiu W, Yan C, Li B, Mo J, Chen J. 2019. Biosynthesis
671 of silver nanoparticles using endophytic bacteria and their role in inhibition of rice
672 pathogenic bacteria and plant growth promotion. *RSC Advances* 9:29293–29299. DOI:
673 10.1039/c9ra04246f.

674 Imoisili PE, Nwanna EC, Jen T-C. 2022. Facile Preparation and Characterization of Silica
675 Nanoparticles from South Africa Fly Ash Using a Sol–Gel Hydrothermal Method. *Processes*
676 10:2440. DOI: 10.3390/pr10112440.

677 Javaid A, Oloketuyi SF, Khan MM, Khan F. 2018. Diversity of Bacterial Synthesis of Silver
678 Nanoparticles. *BioNanoScience* 8:43–59. DOI: 10.1007/s12668-017-0496-x.

679 Jubeh B, Breijyeh Z, Karaman R. 2020. Resistance of gram-positive bacteria to current
680 antibacterial agents and overcoming approaches. *Molecules* 25. DOI:
681 10.3390/molecules25122888.

682 Kalpana D, Lee YS. 2013. Synthesis and characterization of bactericidal silver nanoparticles
683 using cultural filtrate of simulated microgravity grown Klebsiella pneumoniae. *Enzyme and*
684 *Microbial Technology* 52:151–156. DOI: 10.1016/j.enzmictec.2012.12.006.

685 Kalwar K, Shan D. 2018. Antimicrobial effect of silver nanoparticles (AgNPs) and their
686 mechanism – a mini review. *Micro & Nano Letters* 13:277–280. DOI:
687 https://doi.org/10.1049/mnl.2017.0648.

688 Karunakaran G, Jagathambal M, Gusev A, Torres JAL, Kolesnikov E, Kuznetsov D. 2017. Rapid
689 Biosynthesis of AgNPs Using Soil Bacterium Azotobacter vinelandii With Promising
690 Antioxidant and Antibacterial Activities for Biomedical Applications. *JOM* 69:1206–1212.
691 DOI: 10.1007/s11837-016-2175-8.

692 Kumar N, Dubey RC. 2022. Biosynthesis of silver nanoparticles using the endophyte
693 Enterobacter roggenkampii BLS02 from Barleria lupulina and their role in the inhibition of
694 food borne bacteria. *Vegetos*. DOI: 10.1007/s42535-022-00514-z.

695 Kyung JW, Cheong KH, Woo KK, Sook S, Hyun KS, Ho PY. 2008. Antibacterial Activity and
696 Mechanism of Action of the Silver Ion in Staphylococcus aureus and Escherichia coli.
697 *Applied and Environmental Microbiology* 74:2171–2178. DOI: 10.1128/AEM.02001-07.

698 Matras E, Gorczyca A, Przemieniecki SW, Oćwieja M. 2022. Surface properties-dependent
699 antifungal activity of silver nanoparticles. *Scientific Reports* 12:18046. DOI:
700 10.1038/s41598-022-22659-2.

701 Modi S, Yadav VK, Amari A, Osman H, Igwegbe CA, Fulekar MH. 2023. Nanobioremediation:
702 a bacterial consortium-zinc oxide nanoparticle-based approach for the removal of methylene
703 blue dye from wastewater. *Environmental Science and Pollution Research* 30:72641–72651.
704 DOI: 10.1007/s11356-023-27507-y.

705 Murukutti MK, Jena H. 2022. Synthesis of nano-crystalline zeolite-A and zeolite-X from Indian
706 coal fly ash, its characterization and performance evaluation for the removal of Cs+ and Sr2+

707 from simulated nuclear waste. *Journal of Hazardous Materials* 423:127085. DOI:
708 https://doi.org/10.1016/j.jhazmat.2021.127085.

709 Naganthran A, Verasoundarapandian G, Khalid FE, Masarudin MJ, Zulkharnain A, Nawawi NM,
710 Karim M, Abdullah CAC, Ahmad SA. 2022. Synthesis, Characterization and Biomedical
711 Application of Silver Nanoparticles. *Materials* 15. DOI: 10.3390/ma15020427.

712 Pasquina-Lemonche L, Burns J, Turner RD, Kumar S, Tank R, Mullin N, Wilson JS, Chakrabarti
713 B, Bullough PA, Foster SJ, Hobbs JK. 2020. The architecture of the Gram-positive bacterial
714 cell wall. *Nature* 582:294–297. DOI: 10.1038/s41586-020-2236-6.

715 Patel H, Yadav VK, Yadav KK, Choudhary N, Kalasariya H, Alam MM, Gacem A, Amanullah
716 M, Ibrahium HA, Park J-W, Park S, Jeon B-H. 2022. A Recent and Systemic Approach
717 towards Microbial Biodegradation of Dyes from Textile Industries. 14:3163. DOI:
718 10.3390/w14193163.

719 Peiris MMK, Fernando SSN, Jayaweera PM, Arachchi NDH, Guansekara TDCP. 2018.
720 Comparison of Antimicrobial Properties of Silver Nanoparticles Synthesized from Selected
721 Bacteria. *Indian Journal of Microbiology* 58:301–311. DOI: 10.1007/s12088-018-0723-3.

722 Puri N, Gupta A, Mishra A. 2021. Recent advances on nano-adsorbents and nanomembranes for
723 the remediation of water. *Journal of Cleaner Production* 322:129051. DOI:
724 https://doi.org/10.1016/j.jclepro.2021.129051.

725 Rasheed A, Hussain S, Mushtaq W, Zubair M, Siddique K, Attia K, Khan N, Fiaz S, Azeem F,
726 Chen Y. 2023. Application of silver nanoparticles synthesized through varying biogenic and
727 chemical methods for wastewater treatment and health aspects. *Environmental Science and*
728 *Pollution Research*. DOI: 10.1007/s11356-022-24761-4.

729 Raza S, Ansari A, Siddiqui NN, Ibrahim F, Abro MI, Aman A. 2021. Biosynthesis of silver
730 nanoparticles for the fabrication of non cytotoxic and antibacterial metallic polymer based
731 nanocomposite system. *Scientific Reports* 11:10500. DOI: 10.1038/s41598-021-90016-w.

732 Robati D, Mirza B, Rajabi M, Moradi O, Tyagi I, Agarwal S, Gupta VK. 2016. Removal of
733 hazardous dyes-BR 12 and methyl orange using graphene oxide as an adsorbent from
734 aqueous phase. *Chemical Engineering Journal* 284:687–697. DOI:
735 https://doi.org/10.1016/j.cej.2015.08.131.

736 Saeed S, Iqbal A, Ashraf MA. 2020. Bacterial-mediated synthesis of silver nanoparticles and their
737 significant effect against pathogens. *Environmental Science and Pollution Research*
738 27:37347–37356. DOI: 10.1007/s11356-020-07610-0.

739 Saleh MN, Khoman Alwan S. 2020. Bio-synthesis of silver nanoparticles from bacteria Klebsiella
740 pneumonia: Their characterization and antibacterial studies. In: *Journal of Physics:*
741 *Conference Series*. IOP Publishing Ltd,. DOI: 10.1088/1742-6596/1664/1/012115.

742 Sayyid NH, Zghair ZR. 2021. Biosynthesis of silver nanoparticles produced by Klebsiella
743 pneumoniae. *Materials Today: Proceedings* 42:2045–2049. DOI:
744 https://doi.org/10.1016/j.matpr.2020.12.257.

745 Singh PK, Goyal M. 2020. Green Synthesis Using Klebsiella pneumoniae as well as its Execution
746 onto Textiles for Microbe Resistance. In: *IOP Conference Series: Materials Science and*
747 *Engineering*. IOP Publishing Ltd,. DOI: 10.1088/1757-899X/988/1/012071.

748 Singh P, Mijakovic I. 2022. Strong Antimicrobial Activity of Silver Nanoparticles Obtained by
749 the Green Synthesis in Viridibacillus sp. Extracts. *Frontiers in Microbiology* 13.

750 Soltani S, Gacem A, Choudhary N, Yadav VK, Alsaeedi H, Modi S, Patel A, Khan SH, Cabral-
751 Pinto MMS, Yadav KK, Patel A. 2023. Scallion Peel Mediated Synthesis of Zinc Oxide
752 Nanoparticles and Their Applications as Nano fertilizer and Photocatalyst for Removal of
753 Organic Pollutants from Wastewater. *Water (Switzerland)* 15. DOI: 10.3390/w15091672.

754 Srinivasan R, Mathivanan K, Govindarajan RK, Uthaya Chandirika J, Govindasamy C. 2022.
755 Extracellular synthesis of silver nanoparticles by bioluminescent bacteria: characterization
756 and evaluation of its antibacterial and antioxidant properties. *International Nano Letters*
757 12:169–177. DOI: 10.1007/s40089-021-00360-y.

758 Sun SJ, Deng P, Peng CE, Ji HY, Mao LF, Peng LZ. 2022. Extraction, Structure and
759 Immunoregulatory Activity of Low Molecular Weight Polysaccharide from Dendrobium
760 officinale. *Polymers* 14. DOI: 10.3390/polym14142899.

761 Swathilakshmi A V, Abirami S, Geethamala G V, Poonkothai M, Sudhakar C, Albasher G,
762 Alamri O, Alsultan N. 2022. Phytonanofabrication of copper oxide mediated by Albizia
763 amara and its photocatalytic efficacy. *Materials Letters* 314:131911. DOI:
764 https://doi.org/10.1016/j.matlet.2022.131911.

765 Tarekegn MM, Balakrishnan RM, Hiruy AM, Dekebo AH. 2021. Removal of methylene blue dye
766 using nano zerovalent iron, nanoclay and iron impregnated nanoclay – a comparative study.
767 *RSC Advances* 11:30109–30131. DOI: 10.1039/D1RA03918K.

768 Terzioğlu E, Arslan M, Balaban BG, Çakar ZP. 2022. Microbial silver resistance mechanisms:
769 recent developments. *World Journal of Microbiology and Biotechnology* 38:158. DOI:
770 10.1007/s11274-022-03341-1.

771 Tripathi DK, Tripathi A, Shweta, Singh S, Singh Y, Vishwakarma K, Yadav G, Sharma S, Singh
772 VK, Mishra RK, Upadhyay RG, Dubey NK, Lee Y, Chauhan DK. 2017. Uptake,
773 Accumulation and Toxicity of Silver Nanoparticle in Autotrophic Plants, and Heterotrophic
774 Microbes: A Concentric Review. *Frontiers in Microbiology* 8.

775 Vimalanathan AB, Ernest V, Arumugasamy K, Tyagi MG. 2013. Biosynthesis of silver nano-
776 particles by the bacterium Micrococcus luteus. *International Journal of Applied Biology and*
777 *Pharmaceutical Technology* 4:77–83.

778 Wang Z, Chen C, Liu H, Hrynshpan D, Savitskaya T, Chen J, Chen J. 2020. Enhanced
779 denitrification performance of Alcaligenes sp. TB by Pd stimulating to produce membrane
780 adaptation mechanism coupled with nanoscale zero-valent iron. *Science of The Total*
781 *Environment* 708:135063. DOI: https://doi.org/10.1016/j.scitotenv.2019.135063.

782 Wang L, Du Y, Zhu Q, Song J, Ou K, Xie G, Yu Z. 2023a. Regulating the Alkyl Chain Length
783 of Quaternary Ammonium Salt to Enhance the Inkjet Printing Performance on Cationic
784 Cotton Fabric with Reactive Dye Ink. *ACS Applied Materials & Interfaces* 15:19750–19760.
785 DOI: 10.1021/acsami.3c02304.

786 Wang Y, Yang L, Xu J, Xin F, Jiang L. 2023b. Applications of synthetic microbial consortia in
787 biological control of mycotoxins and fungi. *Current Opinion in Food Science* 53:101074.
788 DOI: https://doi.org/10.1016/j.cofs.2023.101074.

789 Wang Y, Zhai W, Cheng S, Li J, Zhang H. 2023c. Surface-functionalized design of blood-
790 contacting biomaterials for preventing coagulation and promoting hemostasis. *Friction*
791 11:1371–1394. DOI: 10.1007/s40544-022-0710-x.

792 Wang Y, Zhai W, Li J, Liu H, Li C, Li J. 2023d. Friction behavior of biodegradable electrospun
793 polyester nanofibrous membranes. *Tribology International* 188:108891. DOI:
794 https://doi.org/10.1016/j.triboint.2023.108891.

795 Wypij M, Jędrzejewski T, Trzcińska-Wencel J, Ostrowski M, Rai M, Golińska P. 2021. Green
796 Synthesized Silver Nanoparticles: Antibacterial and Anticancer Activities, Biocompatibility,
797 and Analyses of Surface-Attached Proteins. *Frontiers in Microbiology* 12.

798 Yadav VK, Amari A, Wanale SG, Osman H, Fulekar MH. 2023. Synthesis of Floral-Shaped
799 Nanosilica from Coal Fly Ash and Its Application for the Remediation of Heavy Metals from
800 Fly Ash Aqueous Solutions. *Sustainability* 15:2612. DOI: 10.3390/su15032612.

801 Yadav VK, Gnanamoorthy G, Ali D, Bera SP, Roy A, Kumar G, Choudhary N, Kalasariya H,
802 Basnet A. 2022a. Cytotoxicity, Removal of Congo Red Dye in Aqueous Solution Using
803 Synthesized Amorphous Iron Oxide Nanoparticles from Incense Sticks Ash Waste. *Journal*
804 *of Nanomaterials* 2022. DOI: 10.1155/2022/5949595.

805 Yadav VK, Inwati GK, Ali D, Gnanamoorthy G, Bera SP, Khan SH, Choudhary N, Kumar G,
806 Chaurasia TP, Basnet A. 2022b. Remediation of Azure A Dye from Aqueous Solution by
807 Using Surface-Modified Coal Fly Ash Extracted Ferrospheres by Mineral Acids and
808 Toxicity Assessment. *Adsorption Science and Technology* 2022. DOI:
809 10.1155/2022/7012889.

810 Yang J, Shojaei S, Shojaei S. 2022. Removal of drug and dye from aqueous solutions by graphene
811 oxide: Adsorption studies and chemometrics methods. *npj Clean Water* 5:5. DOI:
812 10.1038/s41545-022-00148-3.

Yassin MT, Mostafa AAF, Al-Askar AA, Al-Otibi FO. 2022. Synergistic Antibacterial Activity of Green Synthesized Silver Nanomaterials with Colistin Antibiotic against Multidrug-Resistant Bacterial Pathogens. *Crystals* 12. DOI: 10.3390/cryst12081057.

Zhang Y, Zhao M, Huang J, Zhao N, Yu H. 2023. Controllable Synthesis, Photocatalytic Property, and Mechanism of a Novel POM-Based Direct Z-Scheme Nano-Heterojunction α-Fe2O3/P2Mo18. *Molecules* 28:6671. DOI: 10.3390/molecules28186671.

Figure 1

Figure 1

FIGURE 1 Schematic diagram for the synthesis of AgNPs using bacterial supernatant.

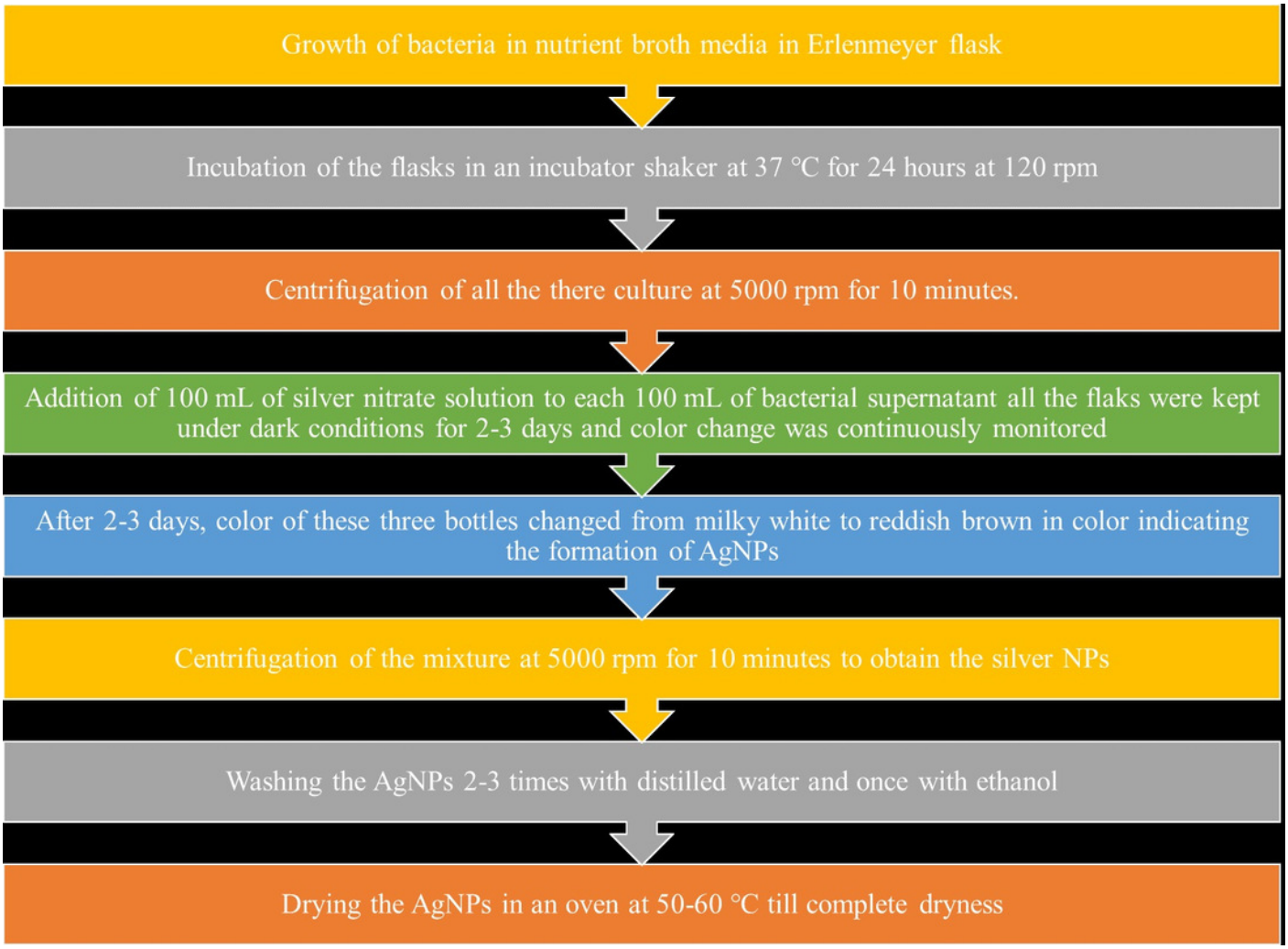

Figure 2

Figure 2

FIGURE 2 Schematic diagram for the formation of AgNPs from silver ions by bacteria via NADH-dependent nitrate reductase enzyme.

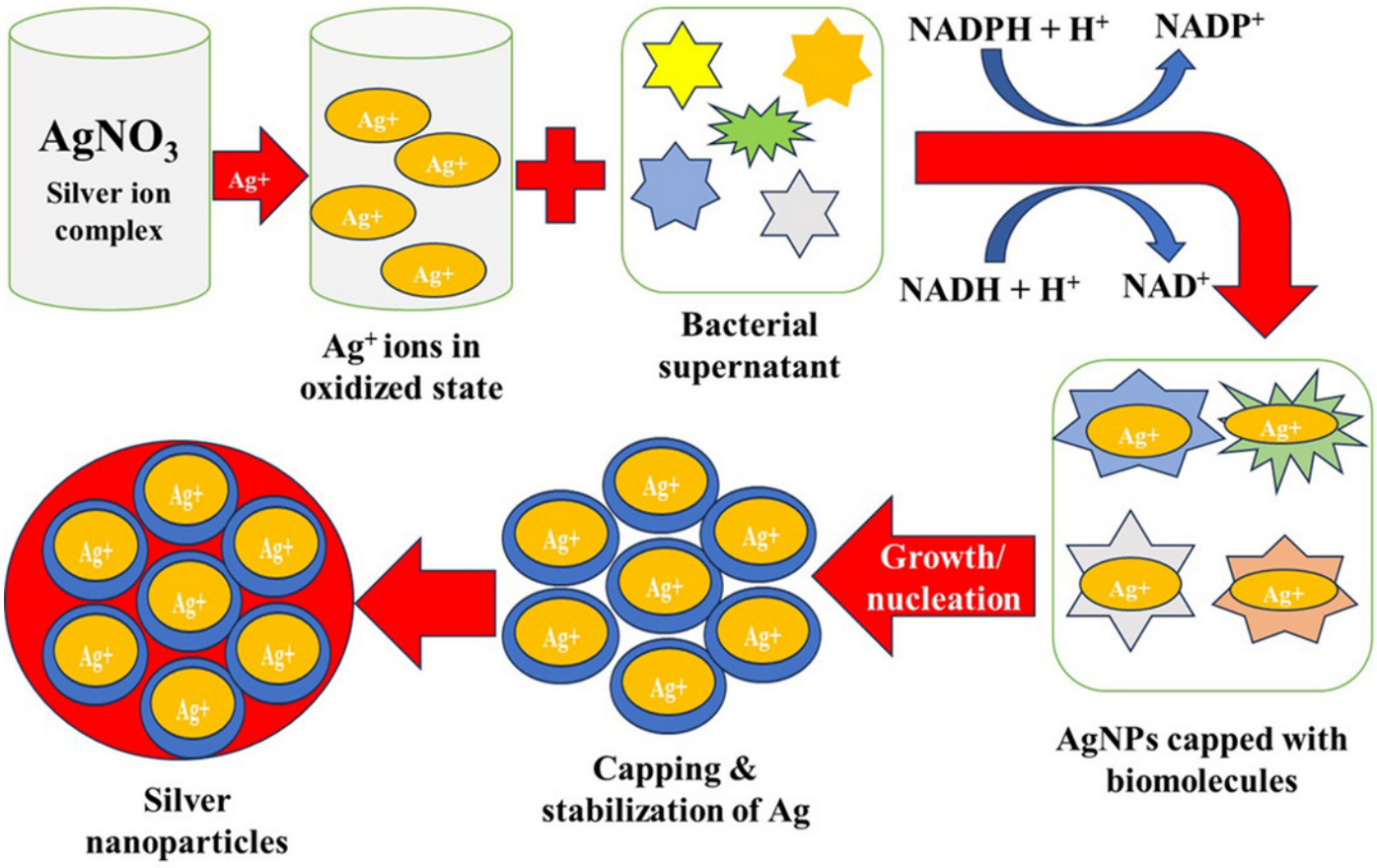

Figure 3

FIGURE 3 UV-Vis measurement of AgNPs synthesized by bacteria.

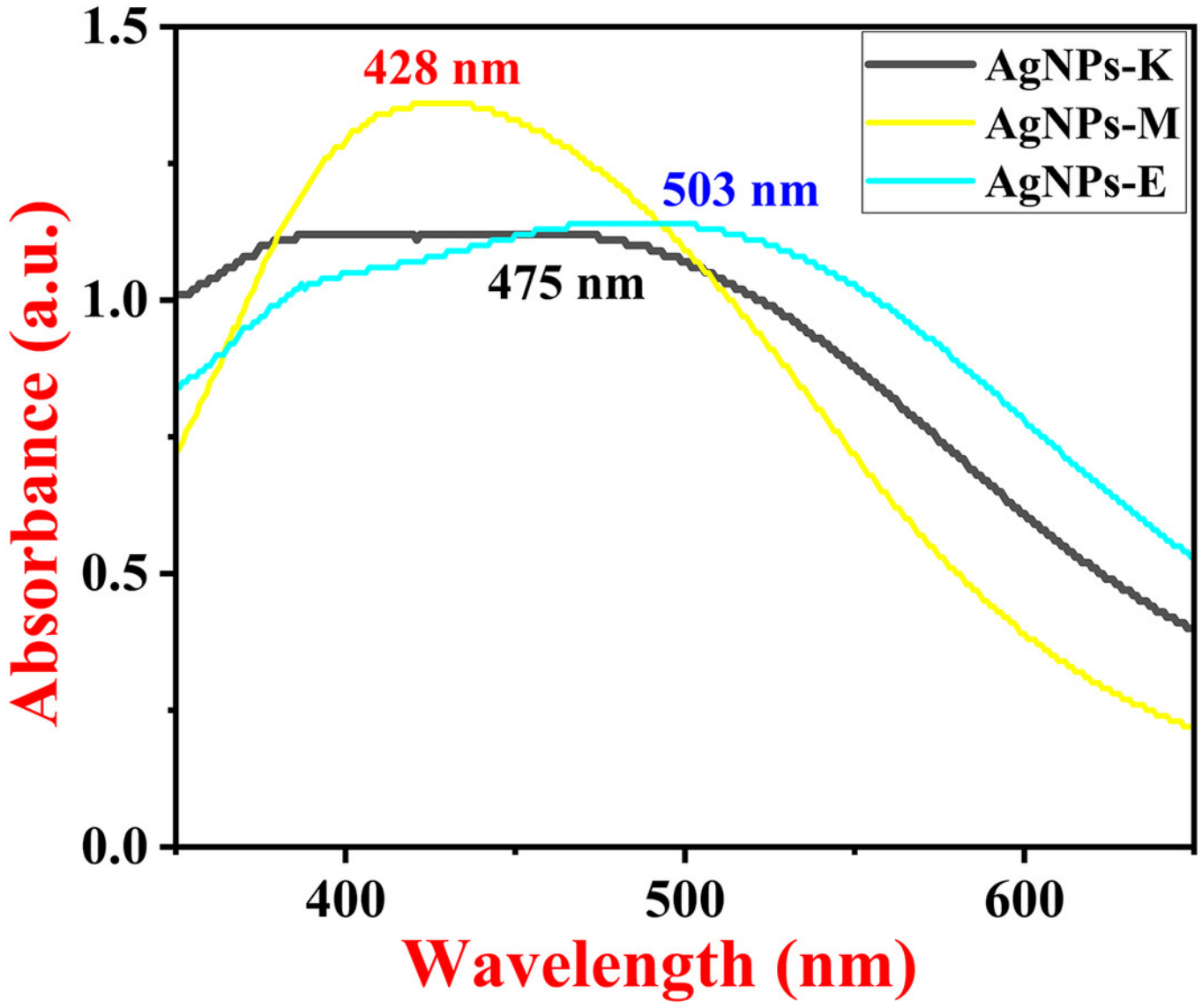

Figure 4

Figure 4

FIGURE 4 FTIR spectra of AgNPs synthesized by bacteria.

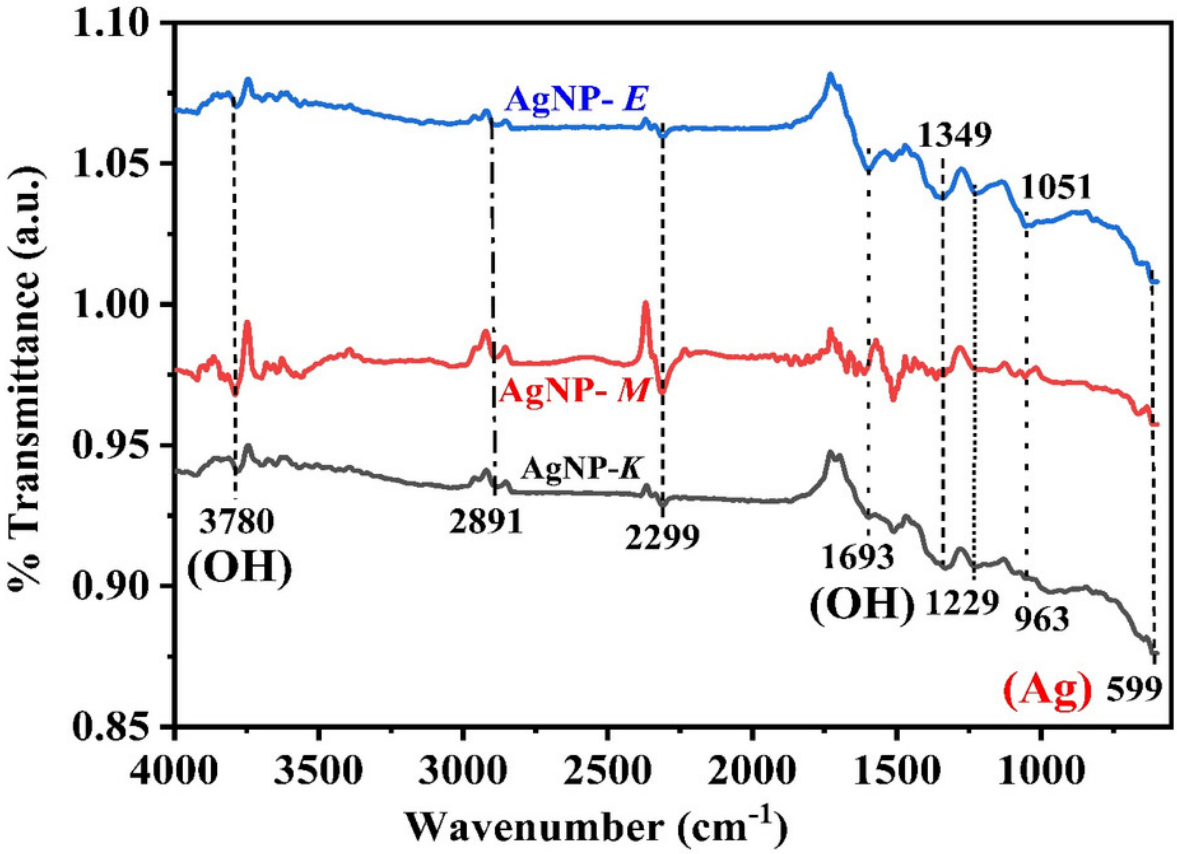

Figure 5

Figure 5

FIGURE 5 XRD pattern of silver nanoparticles synthesized by bacteria.

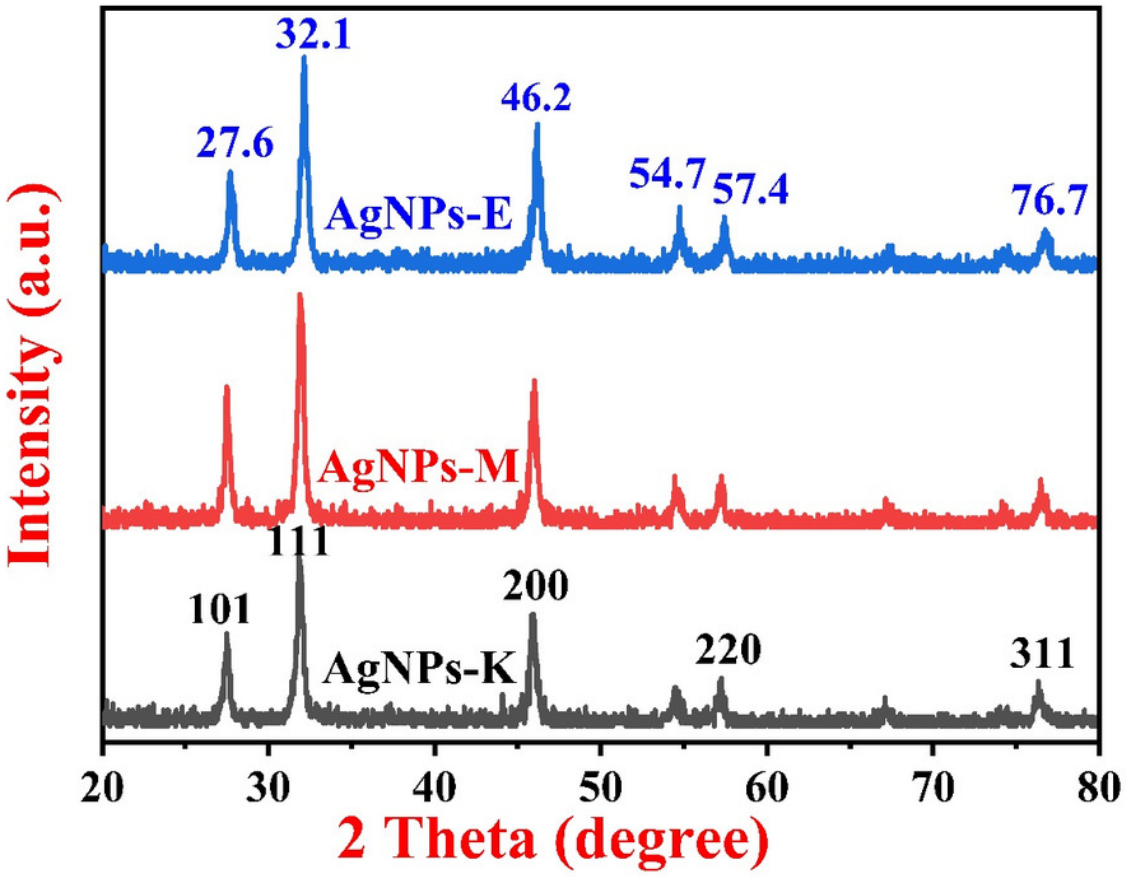

Figure 6

Figure 6

FIGURE 6 FESEM images (a-f), EDS spot (g), and EDS spectra and elemental table (h) for AgNPs-K. FESEM images (i-l), EDS spot (m) and EDS spectra, and elemental table (n) for AgNPs-M. FESEM images (o-r), EDS spot (s) and EDS spectra, and elemental table (t) for AgNPs-E.

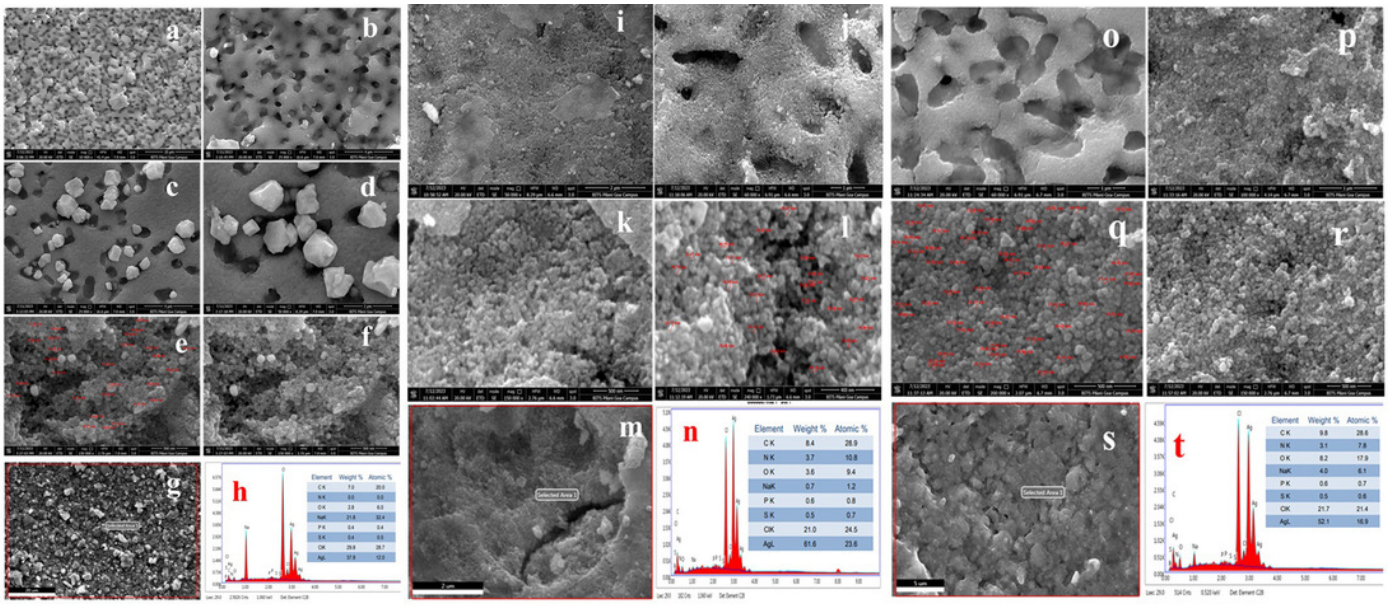

Figure 7

FIGURE 7 MO dye removal by different types of AgNPs with respect to contact time as measured by UV-Vis spectrophotometer: a) AgNPs-K, b) AgNPs-M, and c) AgNPs-E.

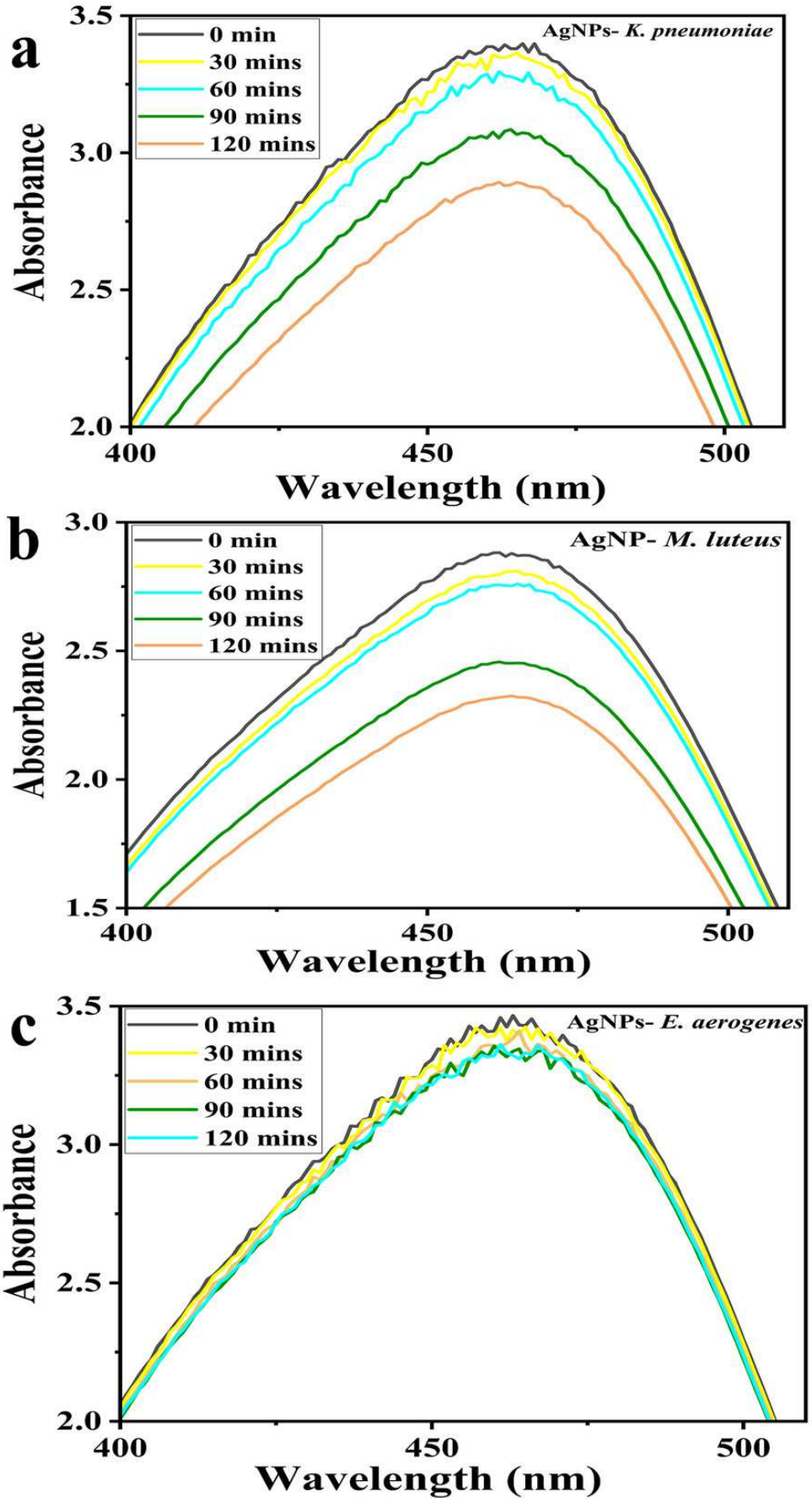
a
AgNPs- K. pneumoniae
0 min
30 mins
60 mins
90 mins
120 mins
Absorbance
Wavelength (nm)
b
AgNP- M. luteus
0 min
30 mins
60 mins
90 mins
120 mins
Absorbance
Wavelength (nm)
c
AgNPs- E. aerogenes
0 min
30 mins
60 mins
90 mins
120 mins
Absorbance
Wavelength (nm)

Figure 8

Figure 8

FIGURE 8 Percentage removal of MO dye by all three types of AgNPs.

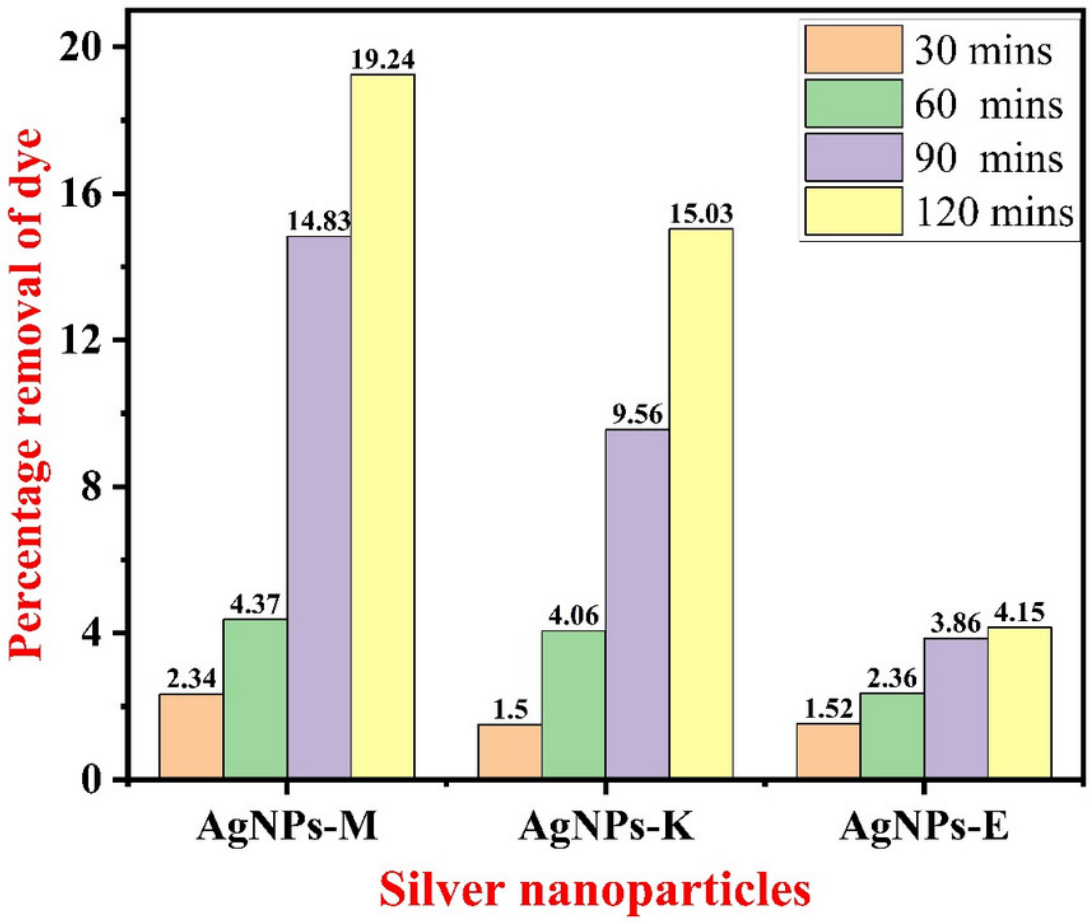

Figure 9

FIGURE 9 Antibacterial activity, zone of inhibition of AgNPs synthesized against the tested bacterial species.

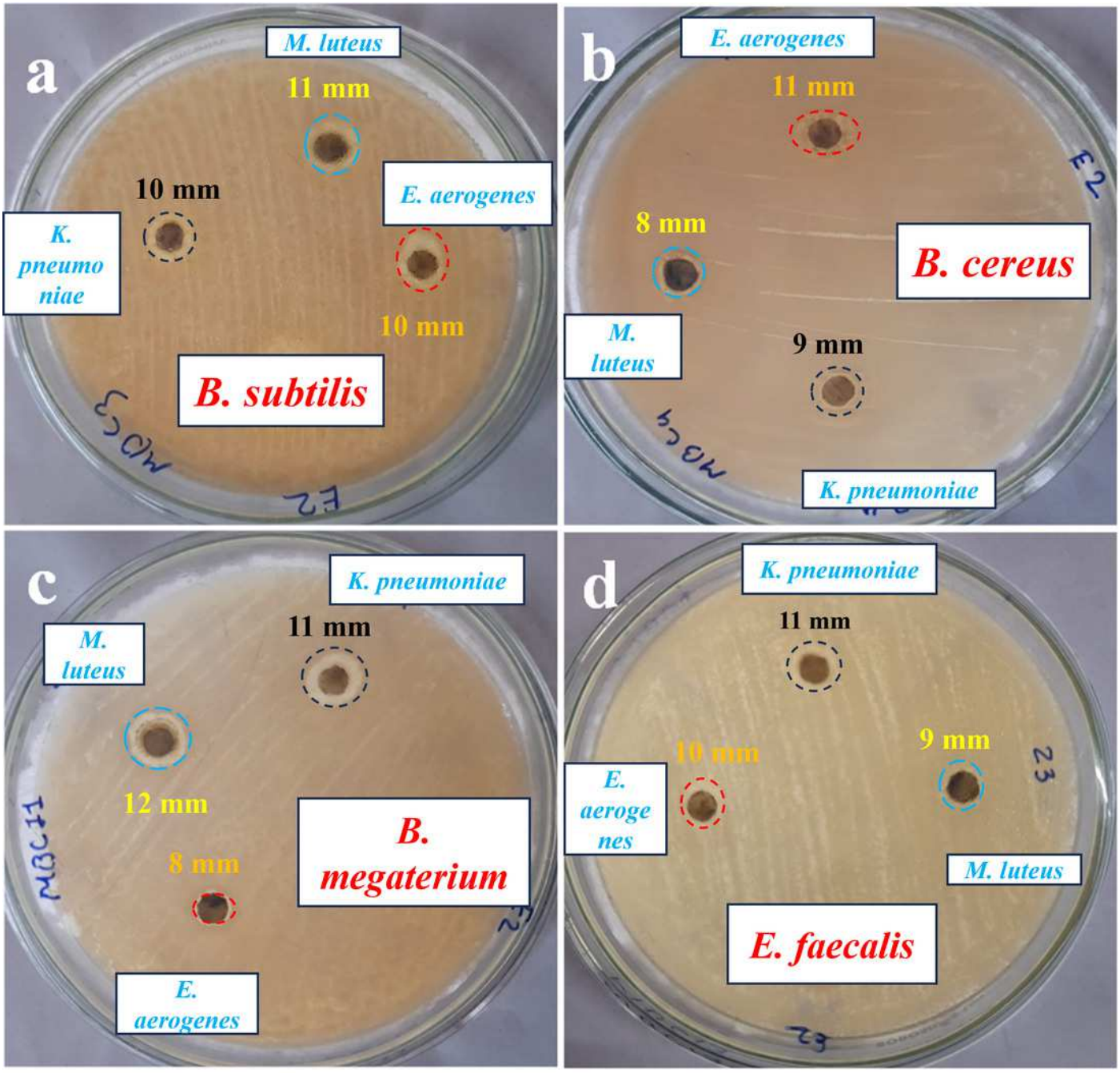

Table 1(on next page)

Table 1

TABLE 1 The major microbial proteins and enzymes present in *K. pneumoniae,* M. luteus, and *E. aerogenes*.

TABLE 1 The major microbial proteins and enzymes present in *K. pneumoniae, M. luteus,* and *E. aerogenes*.

Various microbial proteins and enzymes			
K. pneumoniae	***M. luteus***	***E. aerogenes***	**References**
α-Lactamase	Esterase	α-Lactamase	(Wintachai et al., 2020; Karami-Zarandi et al., 2023)
Lipases	Proteases	Lipases	(Merciecca et al., 2022)
Proteases	Phytases	Proteases	(Wintachai et al., 2020)
Amylases	α-amylase	Amylases	(Pan et al., 2020)
Catalase	Lipases	Catalase	(I & David, 1972)
Gelatinase	-	Gelatinase	(Austin et al., 2020)
Urease	-	Urease	(Carter et al., 2011)
Nitrate reductase			(Singh & Goyal, 2020)
	Dehydrogenases		(Pan et al., 2020)

Table 2(on next page)

Table 2

TABLE 2 Comparison between all the elements present in all three types of AgNPs.

1 **TABLE 2 Comparison between all the elements present in all three types of AgNPs.**

Elements (At. wt.%)	AgNPs- *M. luteus*	AgNPs- *K. pneumoniae*	AgNPs- *E. aerogenes*
Ag	61.6	37.8	52.1
Cl	21.0	29.8	21.7
O	3.6	2.8	8.2
C	8.4	7.0	9.8
Na	0.7	21.8	4.0
N	3.7	0.0	3.1
P	0.6	0.4	0.6
S	0.5	0.4	0.5

2

Table 3(on next page)

TABLE 3 The comparative analysis of all the previous study and current investigation of the bacterially synthesized AgNPs.

TABLE 3 The comparative analysis of all the previous study and current investigation of the bacterially synthesized AgNPs.

Microorganism used for synthesis	Particle size (nm)	Elements observed	Morphology	XRD peaks and crystallite size	Absorbance maxima wavelength (nm)	FTIR bands	References
K. pneumoniae	40.47±89		Cube-shape, irregular heterogeneous forms	-	-	-	(Sayyid & Zghair, 2021)
Pseudomonas aeruginosa ATCC 27853	11.71± 2.73	-	Spherical	-	427	1643, 1586, 1397 and 1042 cm^{-1}	(Peiris et al., 2018)
S. aureus ATCC 25923	11.14± 6.59	-		--	430	2164.86, 2049.17 and 1979.69 cm^{-1}	

E. coli ATCC 25922	13-16	-			420–435	2916.88 cm^{-1}	
Acinetobacter baumannii	8-12	-		-	420–435	1643.75, 2161.48, and 2924.28 cm^{-1}	
K. pneumoniae	5 & 50 (by TEM)	-	Spherical, & triangular (small amount)	37.76°, 45.87°, 64.08° and 77.11° for (1 1 1), (2 0 0), (2 2 0) and (3 1 1)	405–407	2964.55, 1262.22, 1095.89, 1021.96, 800.73, 2960.64, 1650.01, 865.33, 701, 477.07 cm^{-1}	(Kalpana & Lee, 2013)
K. pneumoniae	26.84 to 44.42	-	Cube-shape to heterogeneous, agglomerated	-	432	2115.35,1635.60, 3332.78 & 1096.92, cm^{-1}	(Saleh & Khoman Alwan, 2020)

B. siamensis strain C1	25 to 50 Average: 34±3	Ag (91.8%), Cl (7.5%), S (0.7%)	Spherical	27.81 (101), 32.34 (111), 46.29 (200), 57.47 (220), & 77.69 (311)	409	3385, 2925, 1732, 1645, 1556, 1359, 1079 & 537 cm^{-1}	(Ibrahim et al., 2019)
B. cereus	2-16		Spherical		420		(Gurunathan, 2019)
K. pneumoniae	22-66	Ag, Cl, C, Na, O, S, N & P	Spherical to irregular	27.6, 32.1, 46.2, 54.7, 57.4 % 76.7 Size: 16.88 nm	475	599, 963, 1299, 1349, 1693, 2299, 2891, & 3780 cm^{-1}	Current investigation
M. luteus	21-45	Ag, Cl, C, Na, O, S, N & P	Spherical to irregular	27.6, 32.1, 46.2, 54.7, 57.4 %	503	599, 963, 1299, 1349, 1693, 2299, 2891, &	Current investigation

				76.7 Size: 18 nm		3780 cm^{-1}	
E. aerogenes	24-60	Ag, Cl, C, Na, O, S, N & P	Spherical to irregular	27.6, 32.1, 46.2, 54.7, 57.4 % 76.7 Size: 16.44 nm	428	599, 963, 1299, 1349, 1693, 2299, 2891, & 3780 cm^{-1}	Current investigation

3

Table 4(on next page)

Table 4

TABLE 4 The ZOI, tested bacterial species, against different bacterially synthesized AgNPs.

TABLE 4 The ZOI, tested bacterial species, against different bacterially synthesized AgNPs.

Tested bacteria	Silver nanoparticles (ZOI in mm)		
	AgNPs- K. pneumoniae	***AgNPs- M. luteus***	***AgNPs- E. aerogenes***
B. subtilis	**10**	**11**	**10**
B. cereus	**9**	**8**	**11**
B. megaterium	**11**	**12**	**8**
E. fecalis	**11**	**9**	**10**

Table 5(on next page)

Table 5

TABLE 5 Summarized form of comparison of antibacterial activity of AgNPs of earlier reported work and current investigation.

TABLE 5 Summarized form of comparison of antibacterial activity of AgNPs of earlier reported work and current investigation.

Tested organism	Synthesized by bacteria	Concentration of AgNPs (µg/mL)	Zone of inhibition (mm)	Method applied	References
E. coli, Ps. Aeruginosa, Staph. aureus & *B. cereus*		50	Lowest	Agar-diffusion method	(Saleh and Khoman Alwan, 2020)
		100			
		150	Highest		
Salmonella enterica, *E. coli* & *S. pyogenes*		50 & 100			(Kalpana and Lee, 2013)
		40 to 50 µg/mL			
E. fergusonii	*Bacillus cereus*	MIC: 7.5		Tube dilution method	(Gurunathan, 2019)
S. mutans		MIC: 9.5			
E. coli	*E. coli*		10.0		(Peiris et al., 2018)
Ps. aeruginosa	*E. coli*		10.0		
E. coli	*S. aureus*		14.7		

Ps. aeruginosa			13.0		
Staph. aureus			12.7		
MRSA			12.7		
E. coli	*Acinetobacter baumanii*		13.3		
Ps. aeruginosa			14.7		
E. coli	*P. aeruginosa*		13.0		
Ps. aeruginosa			12.0		
Staph. aureus			12.3		
MRSA			12.7		
B. subtilis	*K. pneumoniae*		10	Agar-well diffusion	Current investigation
B. cereus			9		
B. megaterium			11		
E. fecalis			11		
B. subtilis	*M. luteus*		11		
B. cereus			8		
B. megaterium			12		
E. fecalis			9		

B. subtilis	*E. aerogenes*		10		
B. cereus			11		
B. megaterium			8		
E. fecalis			10		

3